2348
#2

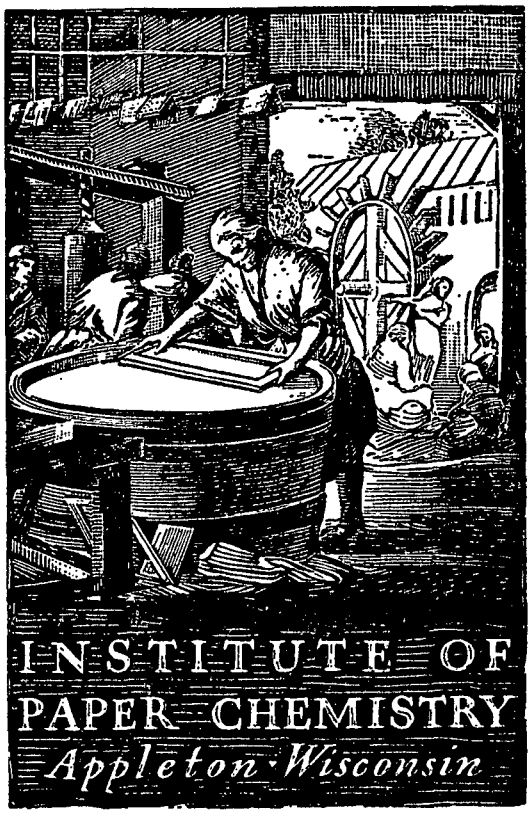


# STUDIES OF THE SHEET-FORMING PROCESS

## Permeation of Thin Fiber Mats

Project 2348

Report Two

A Progress Report

to

MEMBERS OF GROUP PROJECT 2348

March 29, 1963

THE INSTITUTE OF PAPER CHEMISTRY
Appleton, Wisconsin

# STUDIES OF THE SHEET-FORMING PROCESS

## PERMEATION OF THIN FIBER MATS

Project 2348

Report Two

A Progress Report to

MEMBERS OF GROUP PROJECT 2348

March 29, 1963

Members of Group Project 2348:

Consolidated Papers, Inc.
Crown Zellerbach Corporation
Eastman Kodak Company
The Eaton-Dikeman Company
P. H. Glatfelter Co.
International Paper Company
Kimberly-Clark Corporation
KVP Sutherland Paper Company
Longview Fibre Company
Marathon Division, American Can Company
The Mead Corporation
Personal Products Company
Riegel Paper Corporation
St. Regis Paper Co.
Scott Paper Company
Union Bag-Camp Paper Corporation
West Virginia Pulp & Paper Company

TABLE OF CONTENTS

THE INSTITUTE OF PAPER CHEMISTRY
Appleton, Wisconsin

# STUDIES OF THE SHEET-FORMING PROCESS

## PERMEATION OF THIN FIBER MATS

## SUMMARY

In previous investigations (1, 2), fiber and mat properties have been related to fluid properties and flow characteristics, utilizing experimental data for water flow through relatively thick fiber mats with basis weights greater than about 300 g./sq. m. This report presents the initial investigation of water flow through relatively thin fiber mats with basis weights down to about 8 g./sq. m. Two extremes of wire mesh (28 and 100) were chosen for study to represent the range used in practical papermaking operations. In addition, some studies were made of electromesh screens with geometrically flat surfaces. Water permeation data were obtained for preformed dacron fiber mats with velocities from about 1 to 160 cm./sec. A few special runs were made to extend the velocity range up to 450 cm./sec.

The experimental results were found to be in agreement with the previously established flow correlation, within about ±15% for basis weights as low as 50 g./sq. m. At lower basis weights, it was found that measured pressure drops at a given velocity could deviate as much as 30% from those predicted from the correlation because of significant fiber-wire interaction effects. The largest deviations were found for the 100-mesh wire, in which fiber retention during mat formation was essentially complete. In this case, it appeared that the higher measured frictional pressure drops were due primarily to flow convergence (the crowding together and bending of flow lines) in the thin mats because of the presence of the wire structure, and a more uniform porosity in thin mats. It may be possible for two counterbalancing effects also to be present.

The possibility of decreasing mat compression and increasing average pore size with decreasing basis weight would tend to give mat permeabilities higher than the predicted values. Increased permeability because of these two effects may partially mask the extent of lowered permeabilities because of flow convergence in thin fiber mats. The maximum porosity effect may be quantitatively estimated.

In the case of the studies with the coarse 28-mesh wire, the deviations from the correlation were found to be significantly less than those with the 100-mesh screen. Although it had initially appeared from Estridge's theory (3) that fiber retention on the 28-mesh wire would be nearly complete, it was experimentally verified that fiber losses as great as about 20% for thin mats were occurring. Photomicrographs of the thin fiber mats formed on the 28-mesh wire showed an apparently broader pore-size distribution than in the case of mats on the 100-mesh wire. It was hypothesized that this shifting of pore-size distribution toward larger pore sizes was caused by the more nonuniform thin mat structure resulting from incomplete fiber retention. This effect would, of course, tend to minimize the higher pressure drops resulting from flow convergence. Depending on the extent of fiber loss, it is possible to have pressure drops either higher or lower than or in agreement with those predicted from the correlation. It was speculated that the unexpected fiber loss through the 28-mesh screens may have occurred because of a significant wall effect tending to align fibers in the direction of flow.

Attempts to minimize fiber-wire interaction by using geometrically flat electromesh screens were found to be unsuccessful because this type of forming structure led to more extensive flow convergence than did conventional cylindrical woven wires. With electromesh screens, serious deviations from the

correlation were found to occur even for relatively high basis weights of about 100 g./sq. m.

In the case of very thin fiber mats with basis weights less than 10 g./sq. m., the mat thickness is only about 3-7 fiber layers, depending upon compacting pressure. Such mats under fluid drag force compression must approach a nearly uniform porosity. The flow correlation may be corrected for a maximum porosity effect by eliminating the integrating factor resulting from the assumption of a porosity distribution. When this is done, the maximum discrepancy of 30% from the correlation may be reduced to about 15% at low velocities (1 cm./sec.) and 20% at high velocities (160 cm./sec.).

Since the remaining discrepancies at low basis weights are relatively small and may be caused by three interacting effects--flow convergence, decreased mat compressibility, and broader pore-size distribution--and since attempts to isolate any one of these three effects would be extremely difficult and time-consuming, it is felt that further improvement of the flow correlation should not be undertaken at this time. Instead, it is proposed for immediate future work that high-velocity water permeation studies be extended to carefully selected wood pulps. As yet, the flow correlation has been shown applicable to wood pulps only over relatively low pressure drop ranges for purely viscous flow. Attempts will be made to extend permeation studies of wood pulps in the flow ranges where the inertial resistance will become a significant factor. These permeation data will be helpful in the interpretation of the studies proposed in Progress Report One (4) of dynamic drainage of wood pulp slurries. Initially, the effect of incomplete fiber retention on mat structure will be eliminated as a variable by using 100-mesh forming wires.

# INTRODUCTION

## PERMEATION OF THICK MATS

In a recent publication (1) and in the draft of the chapter on permeation under Project 2348 (2), the results of experiments on the flow of water through fiber mats for purely viscous flow (velocities below about 1 cm./sec.) to flow where inertial forces predominate (160 cm./sec.) were summarized. The previous data were correlated using a modified hydraulic radius model which relates fiber and mat properties to fluid properties and flow characteristics. One of the unique features of flow through fiber mats is the ability of fibers to deform under fluid stress, with a resulting porosity gradient throughout the mat structure which depends upon the over-all frictional pressure drop across the fiber mat. To attain a high degree of precision in the experimental data, the contribution of the forming-wire resistance to the over-all pressure drop was minimized by studying relatively thick mats (basis weights from about 300 to 3000 g./sq. m.). A few special runs were made in which the basis weight range was reduced to about 40 g./sq. m. At these low weights, the forming-wire resistance becomes a significant part of the fiber mat resistance, but the flow correlation appeared to be applicable. There were some preliminary indications that at lower basis weights significant deviations of the data from the correlation resulted because of an apparent fiber-wire interaction.

## PERMEATION OF THIN MATS

Since most commercial paper is formed in basis weight ranges of about 10 to 100 g./sq. m., one of the primary objectives of Project 2348 is the study of wet mats in this basis weight range. The most simple and direct experimental results may be obtained from permeation data for carefully preformed fiber mats

of controlled structure. Further, the same idealized conditions outlined in Progress Report One (4) on dynamic drainage were used: mat formation from dilute suspension with complete retention and subsequent determination of pressure drop and velocity data at equilibrium mat compaction. Under these conditions, the previously presented permeation equation (1, 2, 4) is:

$$\frac{\Delta P}{W/A} = \frac{\bar{k}(1 - \bar{\epsilon})vS_v^2\mu}{\bar{\epsilon}^3} U + \frac{b'\sqrt{\bar{k}}vS_v\rho}{\bar{\epsilon}^3} U^2 \qquad (1),$$

where

$\Delta P$ = pressure drop across the mat,

$W/A$ = basis weight of the mat,

$v$ = specific volume of the fiber,

$S_v$ = specific surface of the fiber,

$\mu$ = viscosity of the fluid,

$\rho$ = density of the fluid,

$$\bar{k} = k_1 \frac{\bar{\epsilon}^3}{(1 - \bar{\epsilon})^{1/2}} [1 + k_2(1 - \bar{\epsilon})^3] \qquad (2),$$

$k_1$ = 3.5, and $k_2$ = 57 for cylindrical fibers,

$$\bar{\epsilon} = 1 - (1 - \frac{N}{2})^2 vM(\Delta P)^N \qquad (3),$$

$M$ and $N$ being constants in the compressibility function for a mat of uniform porosity under the mechanical compacting pressure $P$,

$$1 - \epsilon = vMP^N \qquad (4),$$

and

$b'$ = inertial resistance coefficient, 0.1, for cylindrical fibers.

Expressed in a dimensionless form, an average friction factor, $\bar{f}$, and average Reynolds number, $\overline{Re}$, are defined by:

$$\bar{f}' = \frac{\bar{\epsilon}^3 \Delta P}{\sqrt{k}\, v S_v (W/A) \rho U^2} = \frac{\sqrt{k}(1 - \bar{\epsilon}) S_v \mu}{\rho U} + b' = \frac{1}{Re'} + b' \quad (5).$$

Any possible deviations of the experimental results for water permeation through thin mats from this correlation may indicate the influence of the forming-wire structure on the mat behavior. Therefore, most of the experimental data reported in this present study were obtained using two extremes of commercially-used wire mesh of 28 and 100. In addition, a few runs were made with a special forming screen having a geometrically flat surface (electromesh of 25 and 80 count). Some limited data were obtained to extend the velocity range to 450 cm./sec. The fibers chosen for study were smooth, cylindrical, dacron fibers of uniform length and diameter.

## FIBER-WIRE INTERACTION

In permeation studies of compressible fiber mats, the measured frictional pressure drop is obtained over the mat and forming wire. To account for the mat compression, the frictional pressure drop over the mat itself is obtained indirectly by subtracting the pressure drop determined in separate experiments for bare wire. This indirect procedure is necessary because of the obvious experimental difficulty in locating a suitable downstream pressure tap exactly at the mat boundary. In conventional forming wires, the wire diameters are large compared to fiber diameters, and some penetration of the initial fiber deposit into the wire structure is unavoidable. The resultant interacting fiber-wire system may affect the flow through fiber mats in a number of possible ways.

### Flow Convergence

In permeation studies, a nearly flat approach velocity profile is obtained by maintaining turbulent flow in the upstream section of the permeation

tube. In the case of flow through a bare forming wire, the water flow lines must converge as they pass through the porous part of the wire structure. This bending and crowding of the water flow lines will begin some distance upstream from the wire surface. At the very minimum, this convergence of water flow lines would be appreciable for at least an order of one wire diameter upstream. Because the wire diameters are very large in comparison to fiber diameters, the flow lines in a thin fiber mat on a forming wire will likewise show this bending and crowding because of the presence of the wire immediately beneath the mat. This effect would be superimposed on the tortuous flow through the fiber mat alone and would result in an increased velocity gradient in the pores of the mat. The increased velocity gradient must ultimately lead to an increased shear stress acting at the fiber surfaces, which will be evidenced by an increased frictional pressure drop across the fiber mat, as opposed to a hypothetical fiber mat with no supporting wire structure beneath it.

Of course, this effect of converging flow lines was minimized in the earlier work by studying only mats whose thicknesses were very large in comparison to wire diameter. In these cases, the contribution of the initial fiber deposit to over-all pressure drop may justifiably be neglected. One of the primary objectives of the present study is to determine the order of magnitude of this effect and the basis weight range in which it is significant.

Schematically, flow convergence because of the presence of wire is illustrated in Fig. 1. When a thin mat deposit (about 10 g./sq. m.) is placed on the wire, it may be qualitatively seen that some of the flow lines would not be as crowded or bent if it were not for the presence of the wire screen (100 mesh) beneath the mat. The presence of the wire also affects the flow lines approaching a thin mat. In the case illustrated, the wire diameter is roughly

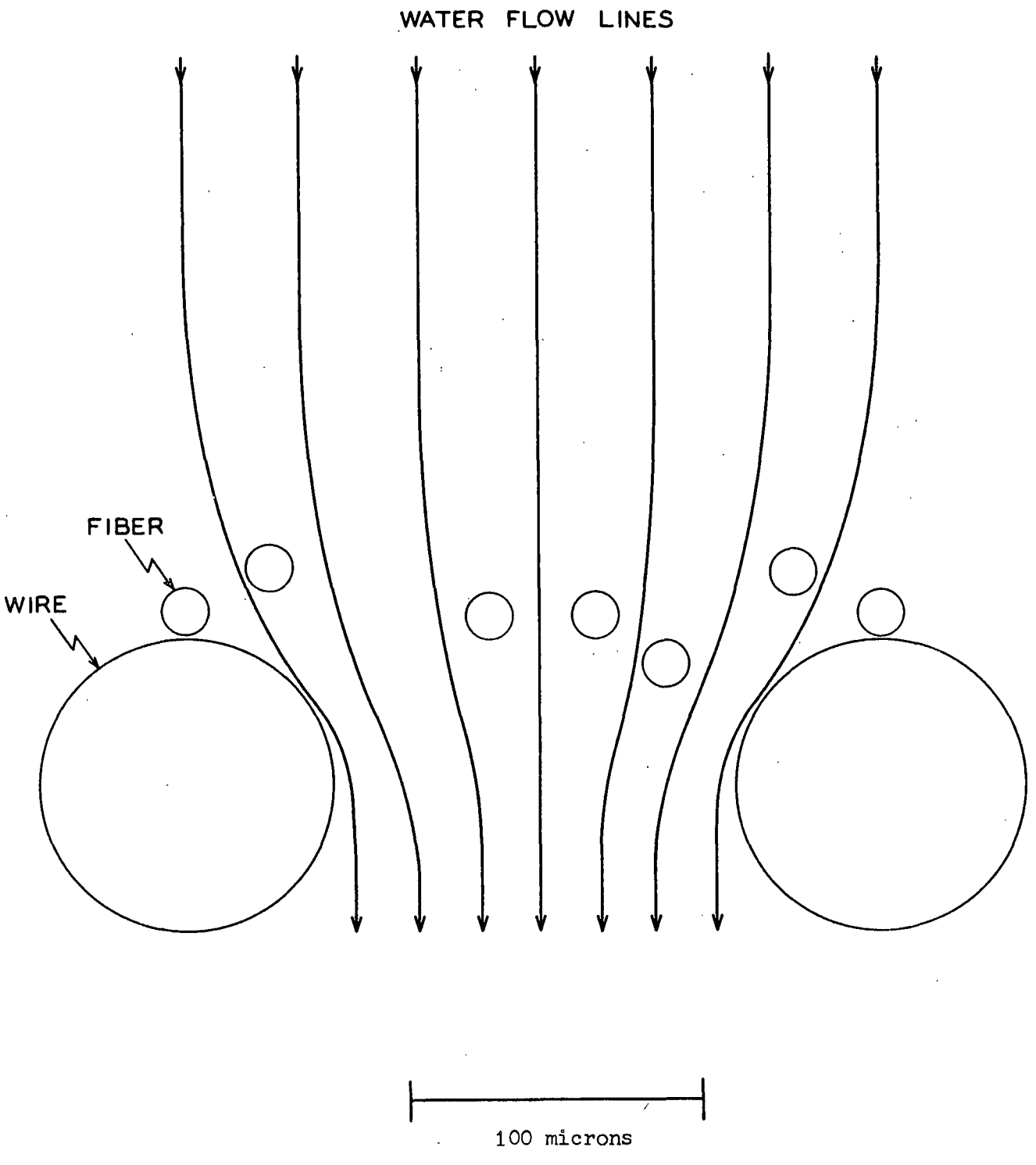


Figure 1. Flow Convergence Because of Presence of Wire

five times as great as the fiber diameter, and the mat has a typically high porosity of about 0.9.

Pore-Size Distribution

Carman (5) and many others have long recognized that the pore-size distribution in a porous medium should have an effect on the permeability coefficient. Carman has carefully pointed out that, in a rigorous sense, a capillary model, or the hydraulic radius model of the Kozeny-Carman theory, is strictly valid only for porous media with a uniform pore-size distribution. He considered a model pore space consisting of nonuniform capillaries such that a group of capillaries with hydraulic radius, $m_i$, accounts for a portion, $\Delta\epsilon_i$, of the pore space. Then the permeability coefficient for viscous flow, $K$, is given by:

$$K = \frac{\epsilon}{k}\overline{(m_i^2)} \tag{6}$$

where, for a continuous pore-size distribution, the average hydraulic radius squared is

$$\overline{(m_i^2)} = \frac{1}{\epsilon}\int_0^{\epsilon} m_i^2 \, d\epsilon_i \tag{7}.$$

In the chapter on permeation (2), it was shown from Parker's data (6) that the permeability calculated from Equations (6) and (7), using a capillary suction technique for determining pore-size distribution, was in approximate agreement with experimentally measured values of permeability coefficient.

Different pore-size distributions may fortuitously give the same permeability coefficient as qualitatively indicated in Fig. 2A. Curve 1 represents

a uniform pore-size distribution, and the permeability coefficient is proportional to the product of $\overline{(\underline{m}_i^2)}$ and $\epsilon$ (the area under the curves). Curve 2 represents the type of pore-size distribution determined by Parker (6) for a synthetic fiber mat, and Curve 3 is an assumed relationship based on a linear pore-size distribution. All three curves are compared at the same porosity, $\epsilon$, and have exactly the same area underneath the curves. Hence, one would expect the permeability coefficient to be the same for these three cases.

On the other hand, there is some indirect experimental evidence based on capillary model reasoning that as fiber mat basis weight is decreased there should be a shifting in both the maximum pore size and the pore-size distribution to larger pores. Qualitatively, this is shown in Fig. 2B, in which Curves 1 to 3 represent decreasing basis weights, respectively. The respective areas under the curves increase, as seen by increasing values of $\overline{(\underline{m}_i^2)}$, indicated by 1' to 3', at the same porosity. Hence, fiber mat permeability should increase with decreasing basis weight. Kallmes and Corte (7), using a gas-drive technique, have shown that the maximum pore size increases with decreasing basis weight.

Physically, the concept of the addition of large pores leading to increased permeability is not difficult to grasp. If small pinholes are made in a thin fiber mat, it is known that the permeability of the mat will decrease because the flow through the large pores overshadows the contribution of the small pores. However, some caution should be observed in interpretation of the quantitative relationships of Equations (6) and (7) since, as previously noted (2), the concept of pore-size distribution is incompatible with the hydraulic radius theory of uniform capillaries.

Figure 3 shows a schematic representation of a thin fiber mat deposit. One can imagine flow occurring through "pores" 1-3. If the basis weight is

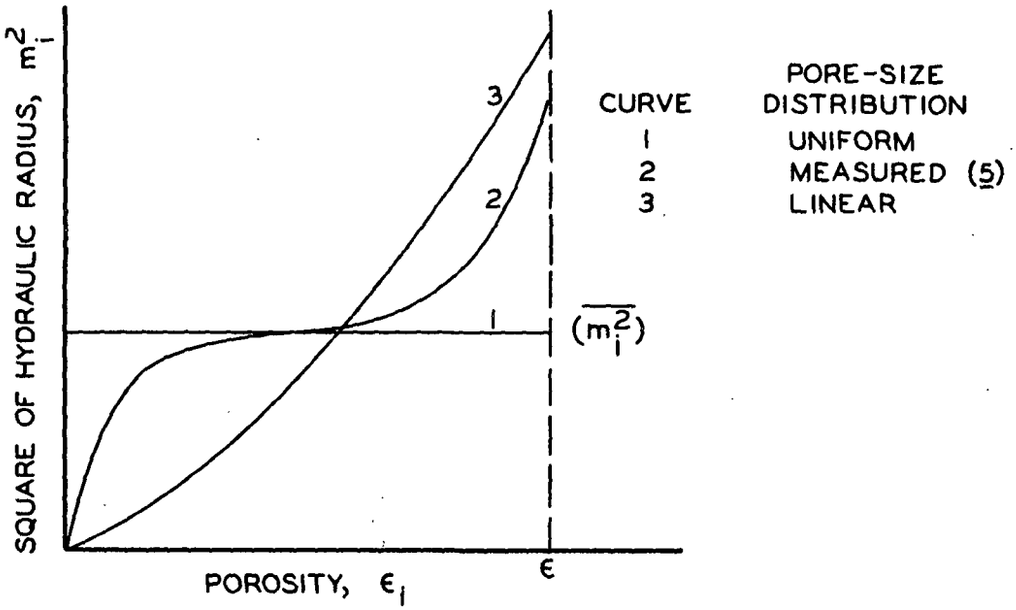


(a) Different Pore-Size Distributions with No Effect on Permeability

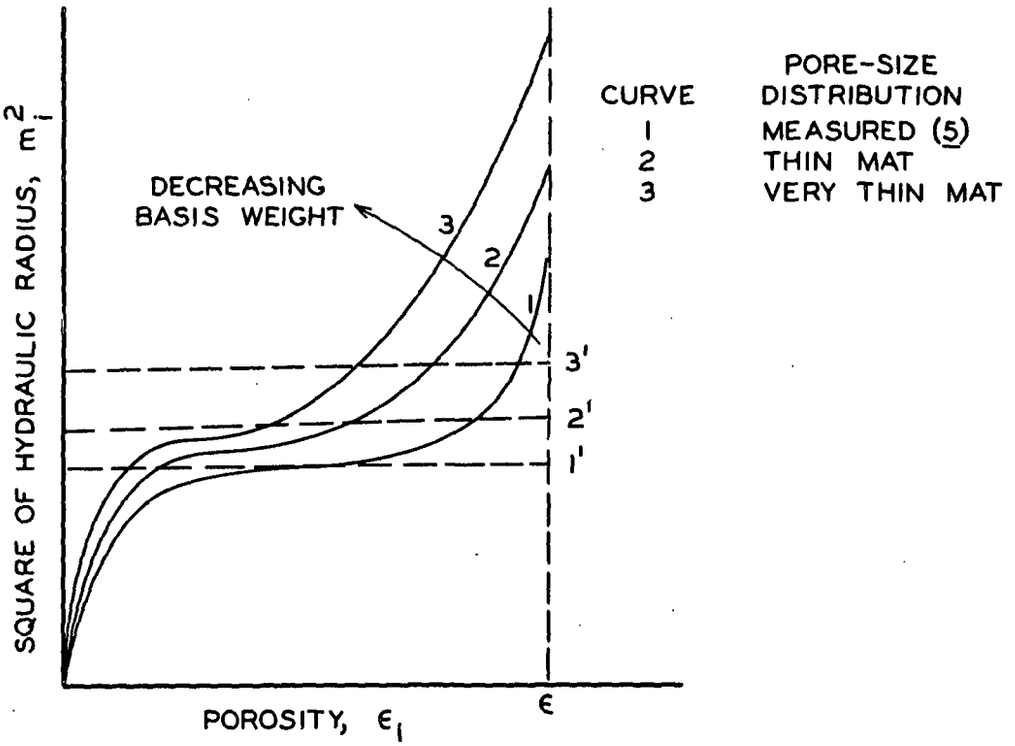


(b) Effect of Basis Weight on Pore-Size Distribution

Figure 2. Effect of Pore-Size Distribution on Permeability

increased by adding the fiber indicated by the dotted lines, the size of "pores" 1 and 2 is decreased, and there should be a subsequent decrease in permeability coefficient. If one visualizes the creation of a pinhole by physical movement of the dotted-line fiber in a direction so as to increase the size of "pores" 1 and 2, the permeability coefficient should be increased.

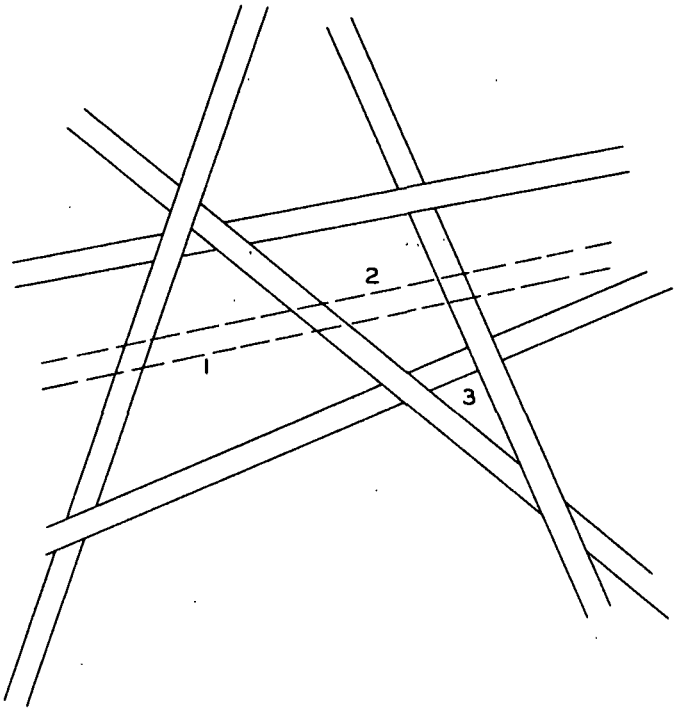


Figure 3. "Pore" Representation in Thin Mat of Synthetic Fibers

In the case of incomplete retention of fibers during the initial formation of the fiber mat, it has been shown by Estridge (3) that a more non-uniform structure results. This nonuniformity in mat structure because of incomplete retention is characterized by larger pore sizes than would be obtained for a more random fiber deposition with complete retention. Hence, here again it would be expected that incomplete retention would lead to higher permeability because of a shifting in pore-size distribution toward larger sized pores.

Porosity Distribution

It has been shown experimentally (8) that a porosity distribution exists in thick mats under fluid stress. Because of the cumulative effect of fluid drag forces, a minimum porosity exists at the forming wire surface with a gradual change to a porosity approaching unity at the mat face where the drag force acting on the fibers is nearly zero. It would be expected, as the thickness of a fiber mat is reduced to only several fiber layers, that the porosity distribution will become more nearly uniform and approach a value corresponding to the over-all frictional pressure drop. A differential layer in a fiber mat has no meaning if it corresponds to a thickness less than one fiber diameter. Hence, in the limit a differential layer corresponds to a mat one fiber diameter thick and with a uniform porosity. For example, in the case of a very thin mat, the average porosity, $\bar{\epsilon}$, of Equation (3) would approach the uniform porosity, $\epsilon$, of Equation (4), in which the compacting pressure, $P$, would be represented by the frictional pressure drop, $\Delta P$.

Therefore, in a thin fiber mat of only several fiber layers' thickness, it would be expected that measured frictional pressure drops would be larger than those predicted from the correlation based on the average porosity concept in Equation (1). The magnitude of this effect may be estimated by using uniform porosities in Equation (1) which are dependent upon compacting pressure equivalent to the over-all pressure drop.

Compressibility

Mat compressibility is empirically correlated by representing the fiber concentration, $c$, as a fractional exponent of compacting pressure, $P$, characterized by the compressibility constants $M$ and $N$ so that

$$c = MP^N \qquad (8).$$

This equation is merely an alternative expression of Equation (4), using fiber concentration instead of fiber solid fraction. As shown by Wilder (9, 10) and Jones (11), the mechanisms of mat compression involve fiber slippage and fiber deformation between points of contact as well as possible fiber deformation at points of contact under high load. It would be expected that as basis weight is decreased to a point where the mat structure becomes only one or two fiber layers thick, the mechanism of fiber slippage would diminish. In the limit for a single layer of fibers, mat compression could take place only because of deformation of individual fibers. Thus, it would be expected that at a certain low value of mat basis weight, the mat would tend to become less compressible until at extremely low basis weights (less than 2 g./sq. m.) the mat would behave almost as an incompressible medium.

This decrease in mat compressibility at very low basis weights would result in a lower pressure drop than would be predicted using the compressibility constants determined for thicker mats.

## PERMEATION TESTER

The flow equipment used to obtain permeation data was essentially the same as that described in previous work (1) for establishment of the flow correlation expressed in Equation (1). Some minor modifications and refinements have been made in the apparatus based on observations made in the earlier work.

### DESCRIPTION OF THE FLOW SYSTEM

Basic requirements of the flow system are to provide a source of pure water at controlled steady-state velocities of about 1-160 cm./sec., and to measure the pressure drop over preformed fiber mats as a function of velocity over a basis weight range of from about 10 to several hundred grams/sq. m. A schematic diagram of the flow apparatus is shown in Fig. 4. The forming section or flow tube was constructed of Lucite, the piping and valves of brass, and the water supply tank, slurry tank, and filters of type 316 stainless steel. The fresh water make-up stored in the supply tank was distilled water prepared from a conventional Barnstead distillation unit supplied with deionized water. The conductivity of the distilled water was about 1 micromho, and the pH was in the range of 5.50 to 5.65. The distilled water was cooled to room temperature by supplying cooling water to the stainless steel coils in the tank. Periodically, the distilled water was reboiled in the supply tank by admitting steam to the coils to remove dissolved air from the water. About once every five days, the supply tank was drained and refilled with freshly distilled water.

The water flows from the supply tank to low- and high-capacity turbine pumps connected in parallel with a combined capacity of about 165 gal./min. Depending upon the desired flow velocity, the system could be operated with

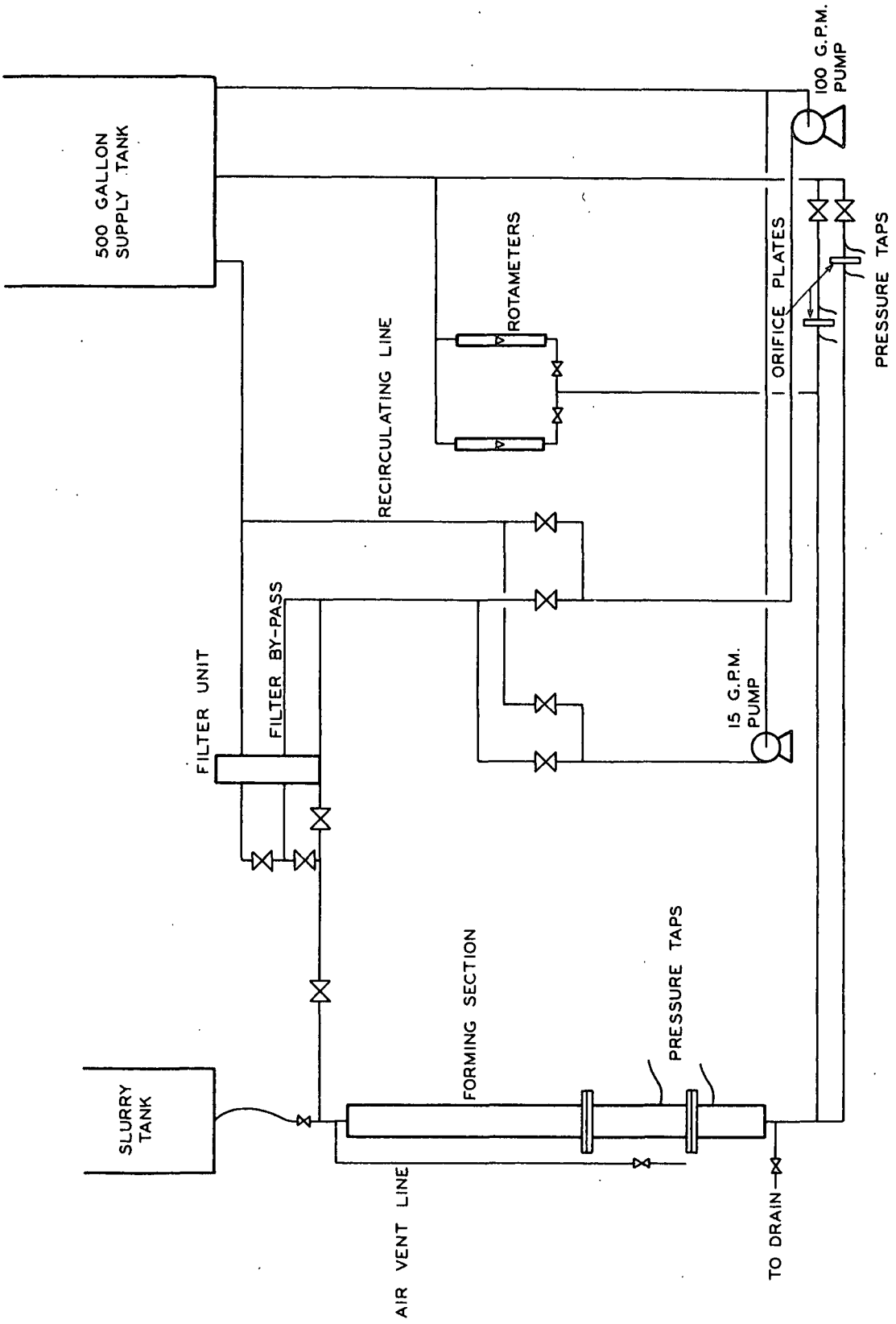


Figure 4. Mat Permeation Flow System

either pump or both in combination. To prevent possible entry of air at the pumps, the bearings on the suction lines were water sealed.

Following the pumps, the water was delivered to a Fulflo filter unit consisting of 18 cotton yarn-wound cylinders supported by stainless steel mesh. The filters were changed periodically when the pressure drop across the unit reached about 20 p.s.i. at maximum flow rate. The rate of water supply to the forming section was controlled by recirculating lines back to the supply tank.

The water flowed from the filtration unit to the upstream part of the forming section, which consisted of flanged Lucite tubing 3 in. i.d. and with a wall thickness of 1/4 inch. The approach section to the forming wire screen was about 1.7 meters and contained a vaned flow straightener to prevent any abnormal velocity distributions. A sketch of the flow straightener is shown in Fig. 5. It consisted of four vertical vanes at right angles to one another and mounted on a conical nose section. The details of the flanged section containing the forming screen with the upstream and downstream pressure taps and pressure-measuring devices are shown in Fig. 6. The forming wires were supported on a perforated brass disk for high pressure drop measurements. In the low pressure drop range, or when using a coarse-mesh wire, the forming wires could be used without the supporting plate. The holes in the brass disk were 1/4 in. in diameter and were spaced to give about 75% open area. In addition, the holes in the upstream section of the plate were countersunk to minimize the land area. The pressure taps in the Lucite tubing were 1/8-in. holes, which were connected to a trap and pulsation damper, and then valved to connect to one of three differential manometers or to a differential pressure gage. The differential manometers were 3 ft. long and were filled with chlorobenzene (sp. gr. 1.105), carbon tetrachloride (sp. gr. 1.585), and mercury (sp. gr. 13.59).

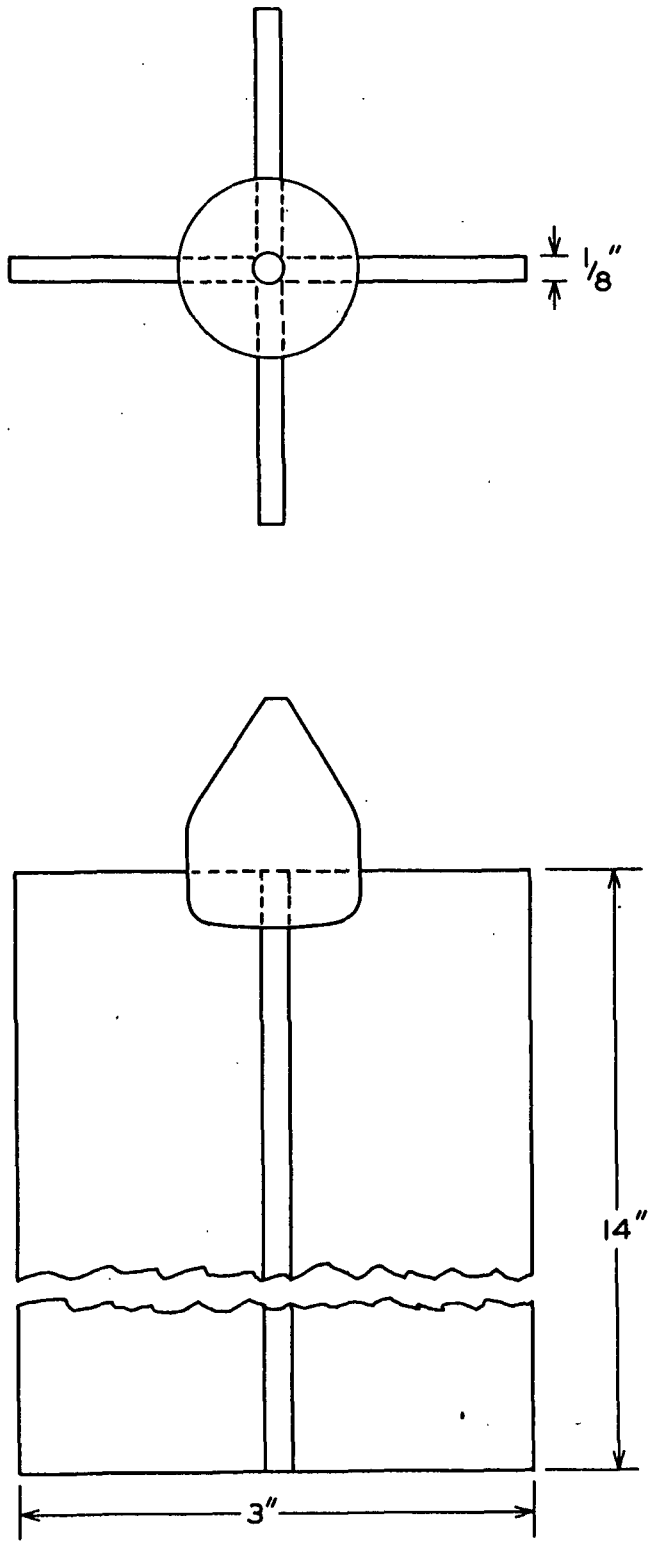


Figure 5. Forming Tube Straightener

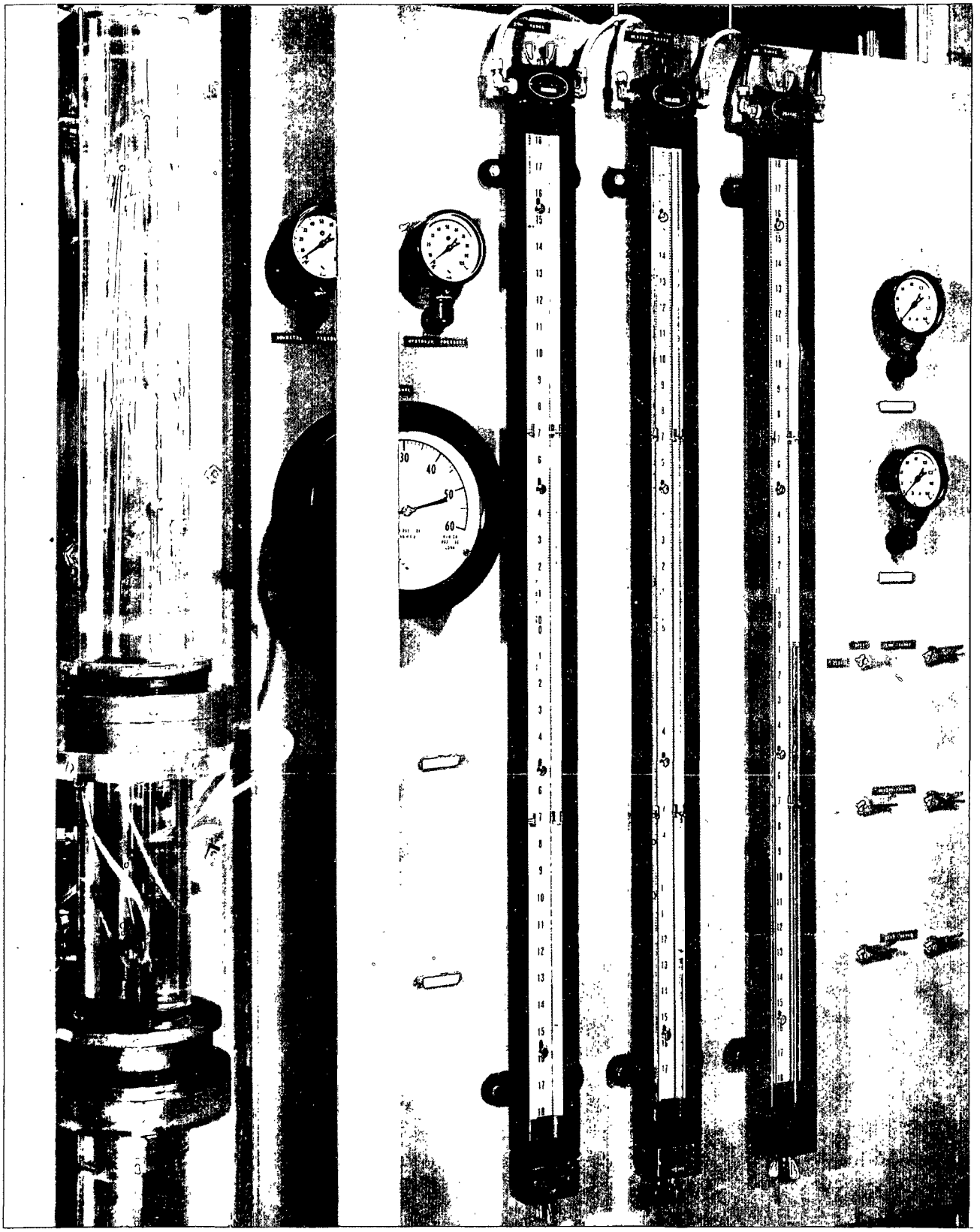

Figure 6. Mat Forming Section and Control Board

The differential pressure gage had a range of 60 p.s.i. The trap leading to the manometer had provision for bleeding air from the system.

The Lucite tubing downstream of the forming wire was about 0.6 m. and was connected to a 3-in. brass well containing a thermometer for water temperature measurement. The flow could then be split to one of two rotameters or one of two orifices for rate measurement. The low-range flow rotameters were used for flow rates up to 10 cm./sec.; the low-range orifice up to 45 cm./sec., and the high-range orifice up to 160 cm./sec. (superficial velocities based on the 3-in. forming section). The metered water was then returned to the supply tank. All the meters were calibrated, and the data compared to the predicted correlation. The agreement of the predictions and calibrated values were within the precision of the meter readings.

MAT FORMATION

The desired fiber weight was dispersed in distilled water and completely deaerated under vacuum. The resulting suspension was added beneath the water surface in the slurry tank of 90-liter capacity and gently agitated with a Lightnin' mixer for five minutes. About 10 drops of a 4% solution of Triton X-100 were added to the slurry tank to decrease the surface tension and prevent fibers from floating to the surface and entraining air. Depending upon the desired mat basis weight, the consistencies in the slurry tank varied from $10^{-4}$ to $10^{-2}$%. The fibers were admitted to the top of the forming section, previously filled with water, by opening the drain valve at the base of the forming section. Mat formation was carried out at a rate of about 1-2 cm./sec. At these velocities, enough turbulence was generated in the upstream part of the forming section to give a nearly flat velocity profile at the forming wire surface. When the desired basis weight was formed (as indicated by the change of level in the slurry

tank), the drain valve was gradually closed while water flow was maintained at the forming velocities by slowly adjusting the low-range rotameter valve. Considerable care was taken during the mat formation procedure to prevent any sudden increases in frictional pressure drop over the mat. During the forming procedure, the mat formation was observed visually through the Lucite tubing, and any unusual fiber motion or flocculation because of small amounts of air entrained on the fiber surfaces was sufficient basis for discarding the run and repeating the forming procedure. The final pressure drop after complete mat formation was recorded, and subsequent permeation testing was carried out at higher pressure drops to prevent hysteresis in mat compression.

TEST PROCEDURES

Following mat formation, the flow rate was adjusted to a desired value and the mat allowed to compress slowly to equilibrium compaction. Roughly, 3 min. were required to reach each flow setting. At equilibrium mat compaction, the frictional pressure drop was read on the appropriate pressure-sensing device, and the temperature was also recorded. The velocity readings were gradually increased and pressure drop and temperature data recorded at each velocity. The water temperature was controlled to $\pm 0.5^{\circ}C$. during any one run at a given basis weight. About 30 separate data points were taken for each run.

At the end of a run, flow was stopped and the forming tube section was drained. Mats were then removed and dried to constant weight at $105^{\circ}C$. Samples of the mat were also taken at the completion of some runs for microscopic examination and for the preparation of photomicrographs.

FIBER CHARACTERIZATION

Smooth, cylindrical dacron fibers were chosen for study. The fibers were supplied in 1/4-in. lengths and were of a specified 3-denier size. The uniformity of individual fiber diameters and lengths were checked microscopically, and the average results were in very close agreement with those calculated from the specifications as shown in Table I. The details of the microscopic measurements are given in Appendix I with photomicrographs of the fibers. The fiber specific surface was based on the weighted average diameter of 17.1 microns ($\underline{S}_{\underline{v}} = 4/\overline{\underline{d}}_{\underline{f}}$).

TABLE I

FIBER PROPERTIES

(3-Denier dacron)

| | |
|---|---|
| Fiber diameter, $\underline{d}_{\underline{f}}$: | |
| Denier, calc. | 17.5 microns |
| Proj. dia., arith. av. | 16.9 microns |
| Surface weighted av.[a] | 17.1 microns |
| Fiber length, $\underline{L}_{\underline{f}}$ | 5.28 mm. |
| Specific volume, $\underline{v}$: | |
| Pycnometric[a] | 0.709 cc./g. |
| Du Pont data | 0.725 cc./g. |
| Specific surface[b], $\underline{S}_{\underline{v}}$: | 2340 sq. cm./g. |
| Compressibility constants: | |
| $\underline{M}$ | 0.00660 c.g.s. units |
| $\underline{N}$ | 0.254 c.g.s. units |

[a] Values chosen for subsequent calculations.

[b] Based on surface weighted av., $\underline{S}_{\underline{v}} = 4/\overline{\underline{d}}_{\underline{f}}$.

Experimental measurements of the fiber densities were made with a pycnometer designed especially for fiber suspensions (Appendix I). The measured density was in good agreement with manufacturer data, as seen in Table I, and the experimental value of 1.41 g./cc. was used in subsequent calculations.

Wet mat compressibilities were measured by means of a static compression technique (12) over the range of 10-5000 cm. of water. The data were correlated by the empirical relationship given in Equation (8). Figure 7 shows a graphical representation of the compression data. The data points shown are average values of duplicate runs. The precision of the measurements was excellent, with an average deviation of less than 2%. The empirical compressibility constants M and N are given in Table I.

FORMING WIRE PROPERTIES

A very coarse 28-mesh wire and a fine 100-mesh wire of plain weave were used for the majority of the permeation studies in this report. It was felt that these two meshes would represent extremes in wires of commercial interest. Wire dimensions and properties were measured and calculated as previously outlined (13), and the results are summarized in Table II. In addition to the above plain-weave wires, two electromesh screens were chosen for study because of their geometrically flat surfaces. It was hoped that the flat surfaces would minimize fiber penetration into the wire structures. The screens were supplied by the C. O. Jelliff Manufacturing Corporation and were produced by electrical etching of a flat plate. Properties of the electromesh screens are summarized in Table II. Photomicrographs of the screens are shown in Appendix II.

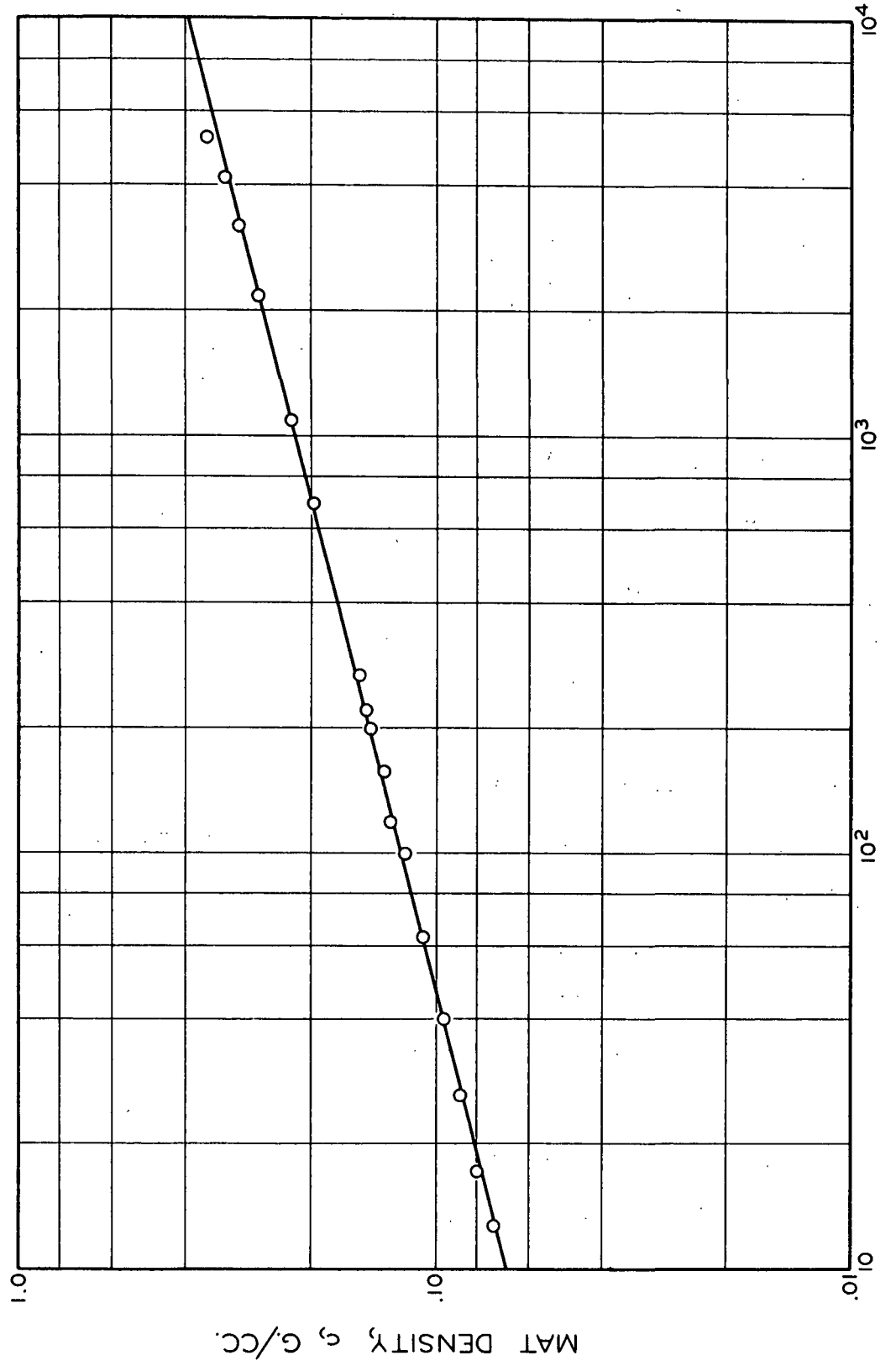


Figure 7. Dacron Fiber Mat Compressibility

TABLE II

WIRE PROPERTIES

| Plain-Weave Wire | Wire Diameter, in. | Wire Thickness, in. | Porosity[a], $\epsilon$, dimensionless |
|---|---|---|---|
| 28 mesh | 0.0155 | 0.0325 | 0.675 |
| 100 mesh | 0.0045 | 0.0098 | 0.675 |

| Electromesh Screen, hole/in. | Aperture Size, in. | Distance Between Apertures, in. | Wire Thickness, in. | Porosity[b], $\epsilon$, dimensionless |
|---|---|---|---|---|
| 25 count | 0.0228 | 0.0194 | 0.0090 | 0.50 |
| 80 count | 0.00692 | 0.0055 | 0.0036 | 0.51 |

[a] Calculated.

[b] Measured by water displacement.

## PERMEATION RESULTS

The experimental permeation data are presented in this section of the report in two ways: (1) Pressure drop is shown as a function of velocity for parameters of basis weight, and (2) all the data are reduced to a single function by relating the dimensionless friction factor and Reynolds number. The pressure drop and velocity data are shown as solid-line curves, and in each case are compared to values calculated from the correlation given in Equation (1) and shown as dashed-line curves. The original pressure drop readings must first be corrected for the pressure drop over the forming wire or screen, and these data were obtained for the bare wires and screens.

### FORMING WIRE RESISTANCES

Pressure drop and velocity curves of the plain-weave wires are shown in Fig. 8, and the electromesh data are shown in Fig. 9. The 28-mesh wire resistances were obtained for the plain wire and for the wire in combination with the perforated backing plate. The 100-mesh wire resistance includes the backing plate. The electromesh screens were rigid enough so that the backing plate was not necessary.

The data from Fig. 8 and 9 were used to calculate the pressure drops over the fiber mats by subtracting the pressure drop of the bare wire from the measured over-all pressure drops over the mat and wire in combination. To facilitate the calculation of pressure drop over the wire at given velocities, the data were fitted to a correlation suggested in a previous study (13), and these empirical relationships are given in Appendix II.

Data for the permeation of the bare screen were obtained at water temperatures of from 19 to 35°C. However, no measurable effect of viscosity

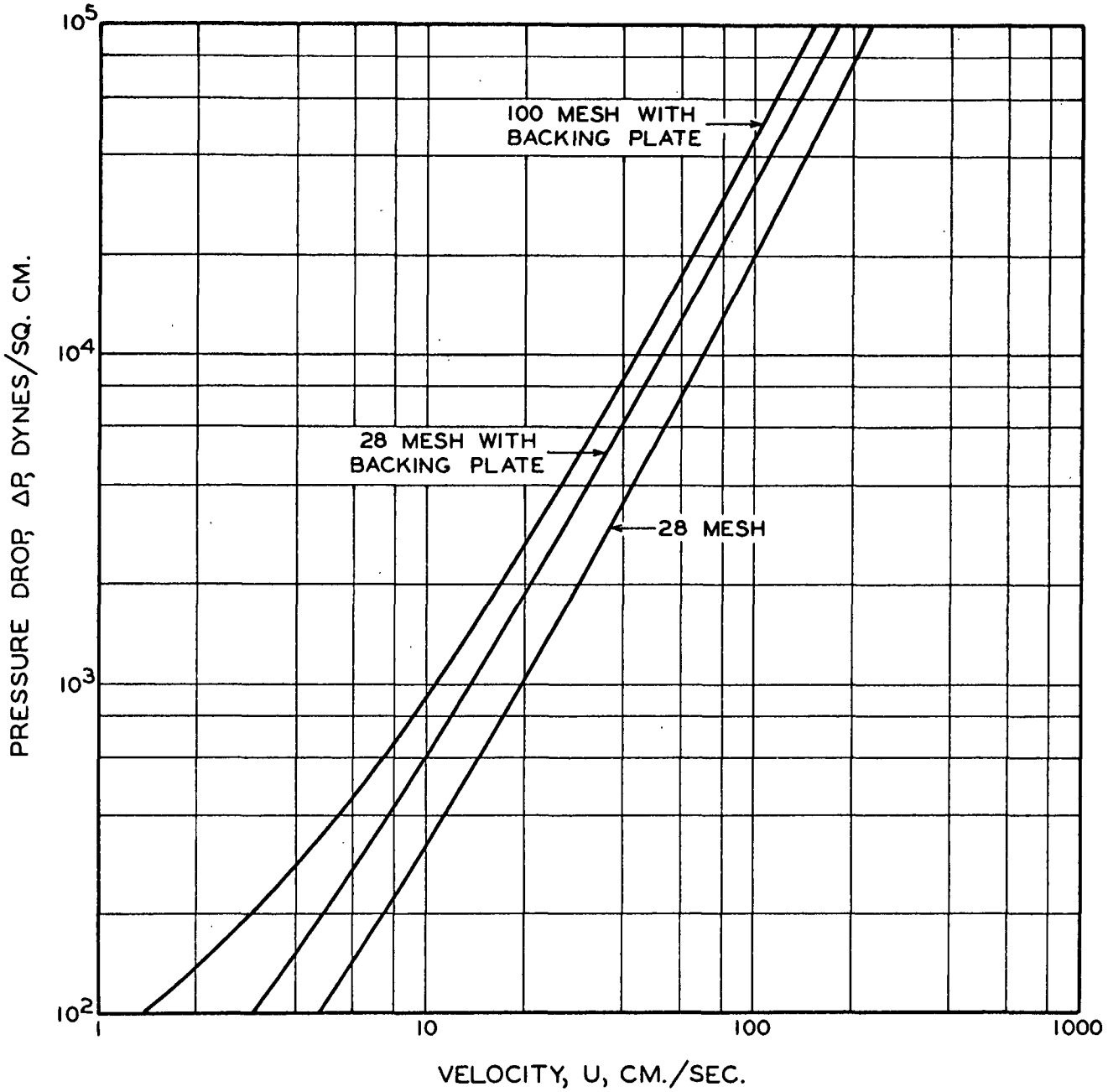


Figure 8. Flow Resistance of Plain-Weave Wires

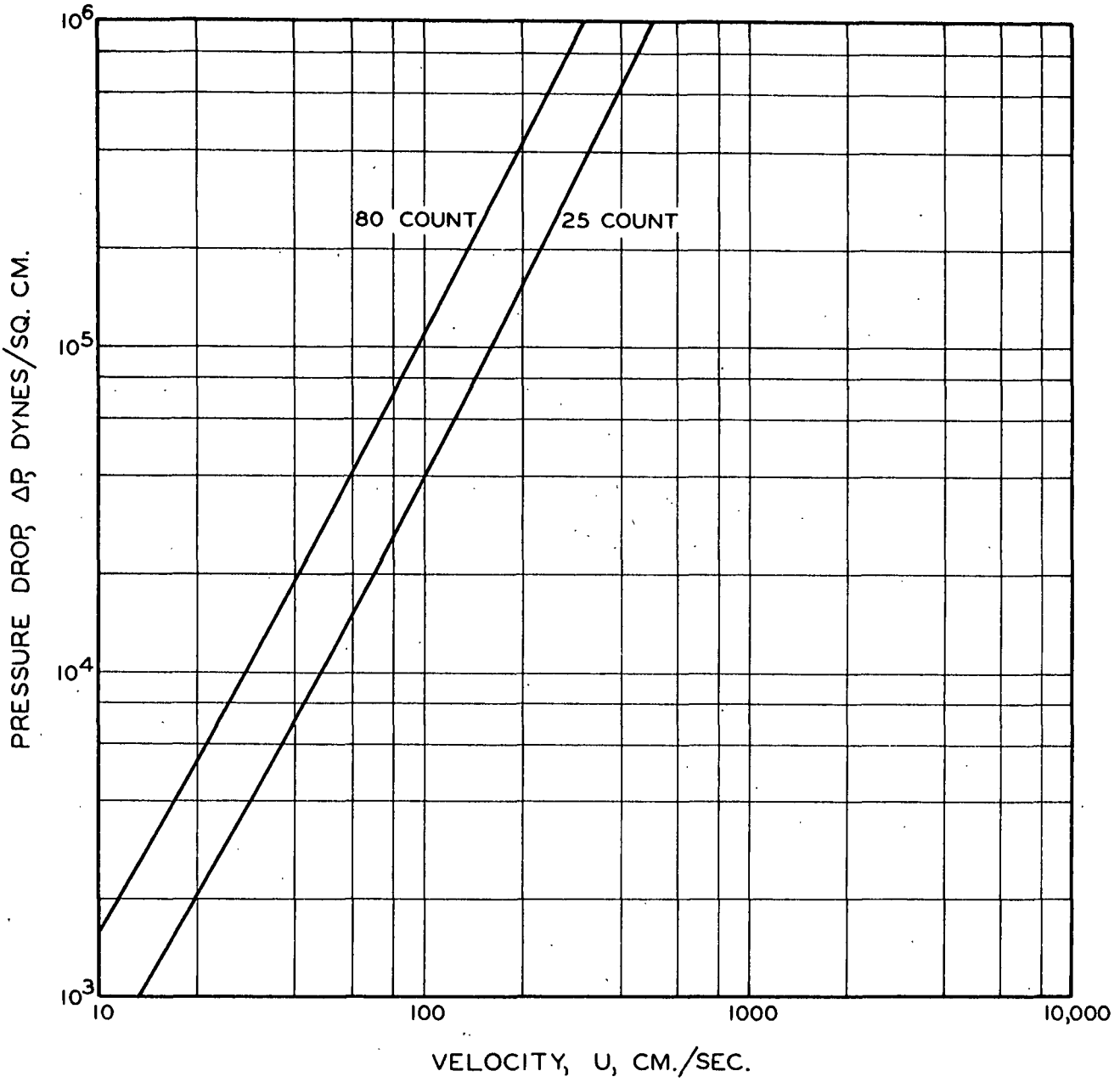


Figure 9. Flow Resistance of Electromesh Screens

was discernible because of the predominance of the inertial resistance over the viscous resistance in the flow ranges studied.

## THIN MAT RESISTANCES

### Pressure Drop-Velocity Data

The data for four mats of basis weights from 13 to 88 g./sq. m. formed on a 100-mesh wire with backing plate are shown in Fig. 10. Marked discrepancies from the correlation are evidenced at basis weights below 50 g./sq. m.

The 28-mesh with backing plate data for seven basis weights from 14 to 320 g./sq. m. are shown in Fig. 11. At the lowest basis weights, the deviations from the correlation are seen to be less than in the previous 100-mesh data. Some deviations from the correlation are seen at higher basis weights but are within the $\pm 10\%$ precision of the correlation.

Next, the results for 28 mesh with no backing plate are given in Fig. 12 for four basis weights from 8 to 65 g./sq. m. In this case, the low basis weight data are in agreement with the correlation, and deviations from the correlation at higher basis weights are not considered significant.

### Friction Factor Correlation

All the data presented in Fig. 10-12 are shown in Fig. 13, where friction factor is plotted as a function of Reynolds number as defined in Equation (5). Values predicted from the correlation are indicated by the solid-line curve, and the dotted-line curves show a $\pm 15\%$ deviation zone. Most of the data points falling outside the $\pm 15\%$ deviation limit are those from mats formed on the 100-mesh wire at basis weights below 50 g./sq. m. It may be concluded that the correlation predicts the flow characteristics within $\pm 15\%$

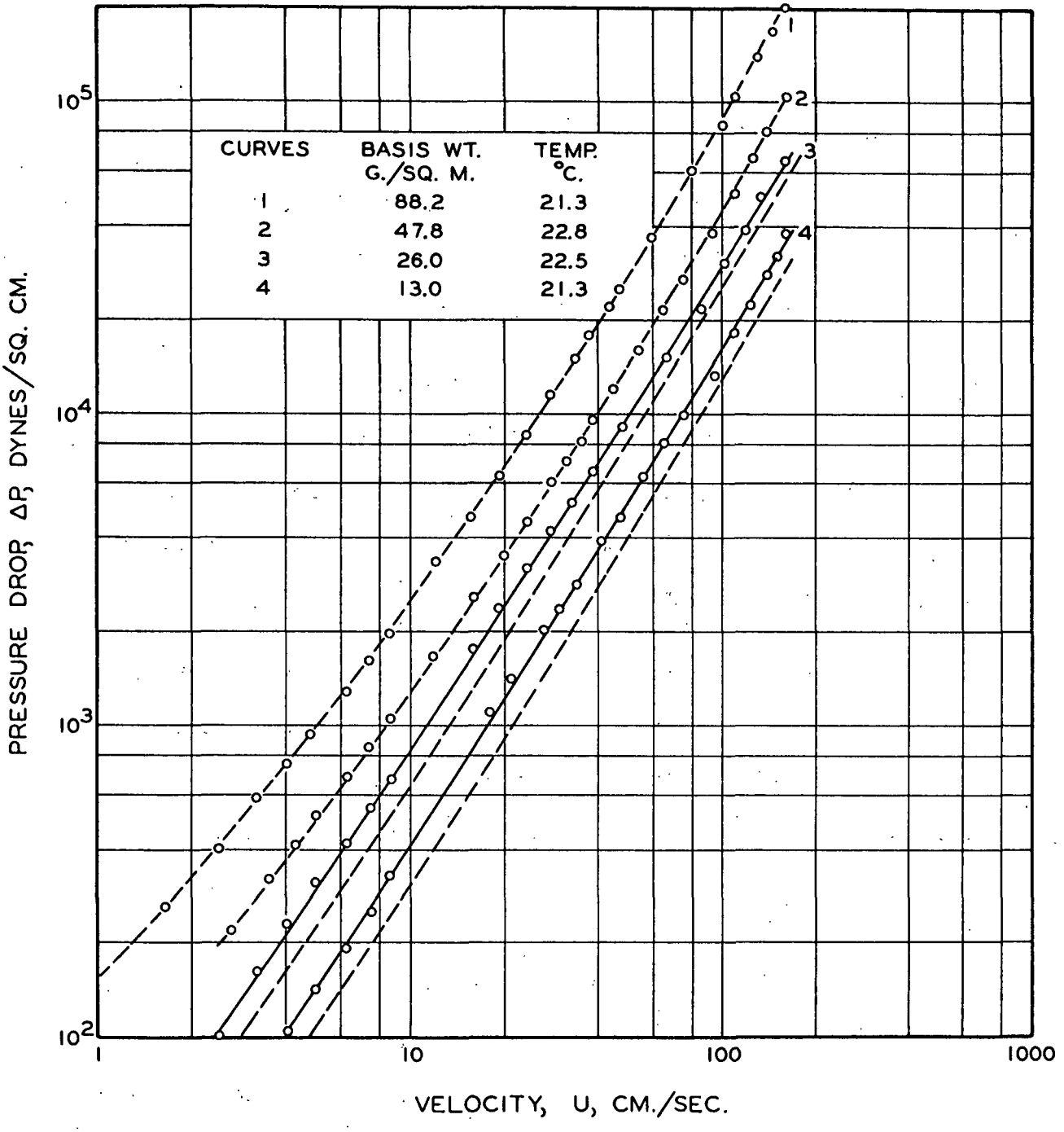


Figure 10. Flow Resistance of Mats on 100-Mesh Wire (with Backing Plate)

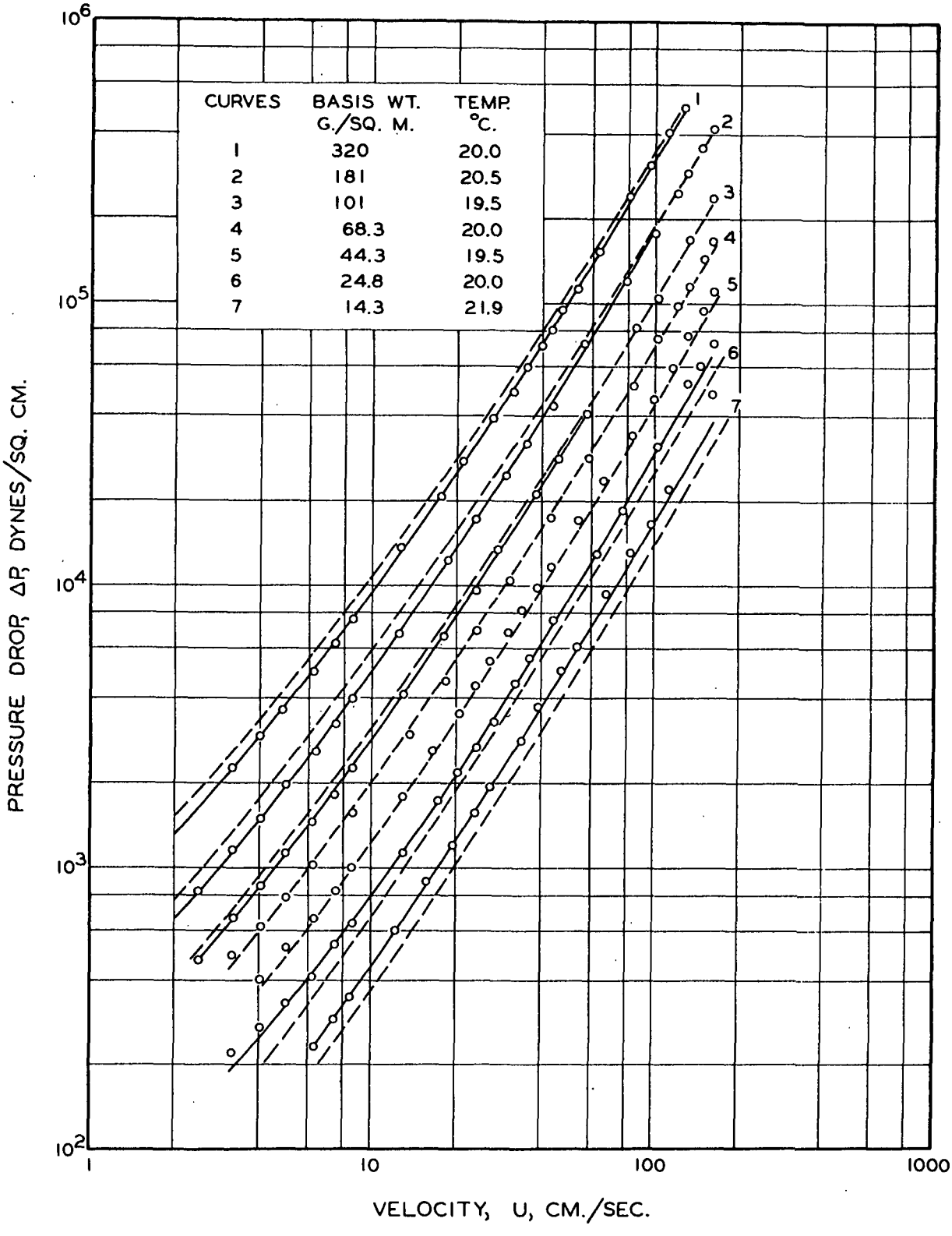


Figure 11. Flow Resistance of Mats on 28-Mesh Wire (with Backing Plate)

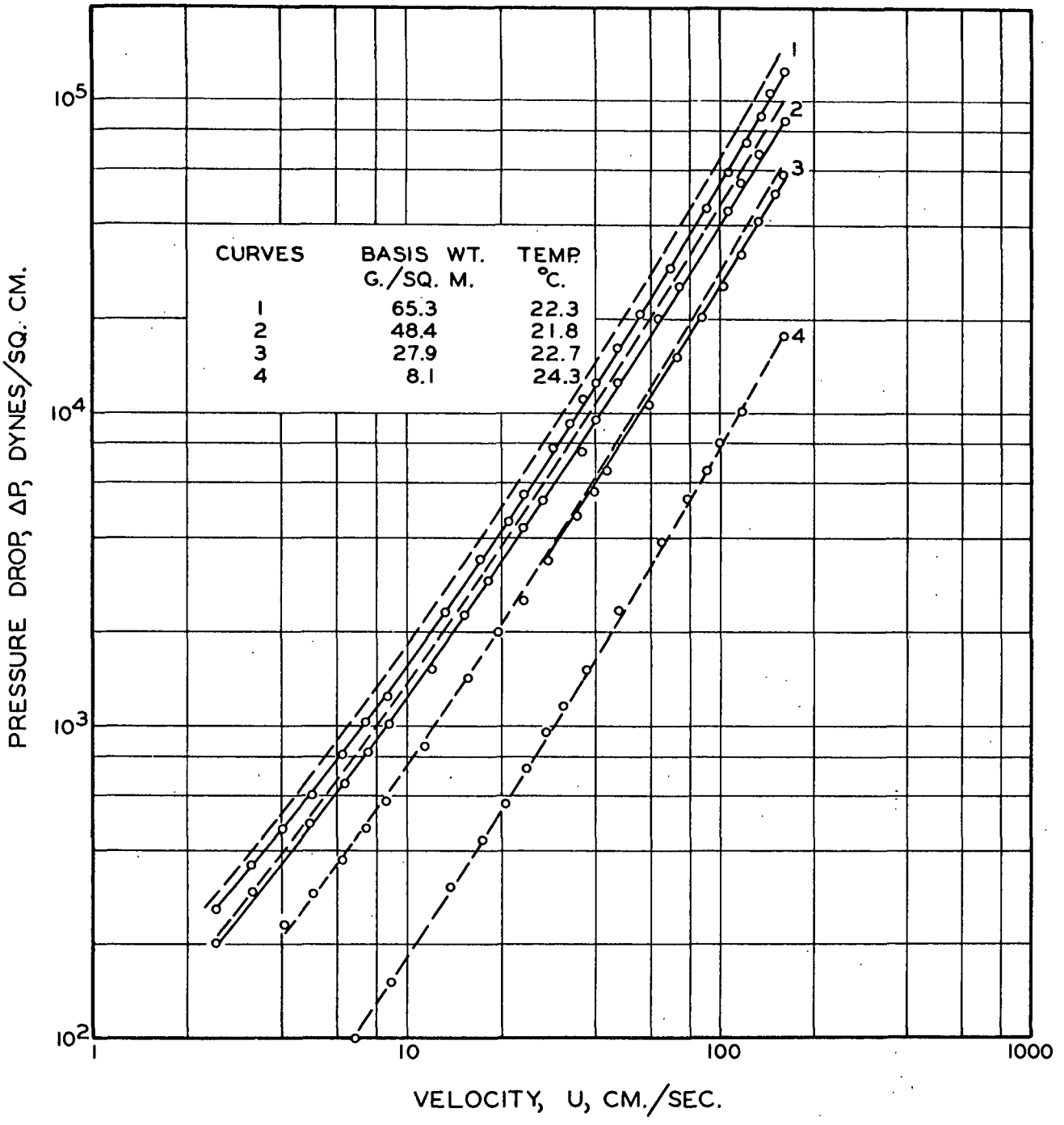


Figure 12. Flow Resistance of Mats on 28-Mesh Wire (No Backing Plate)

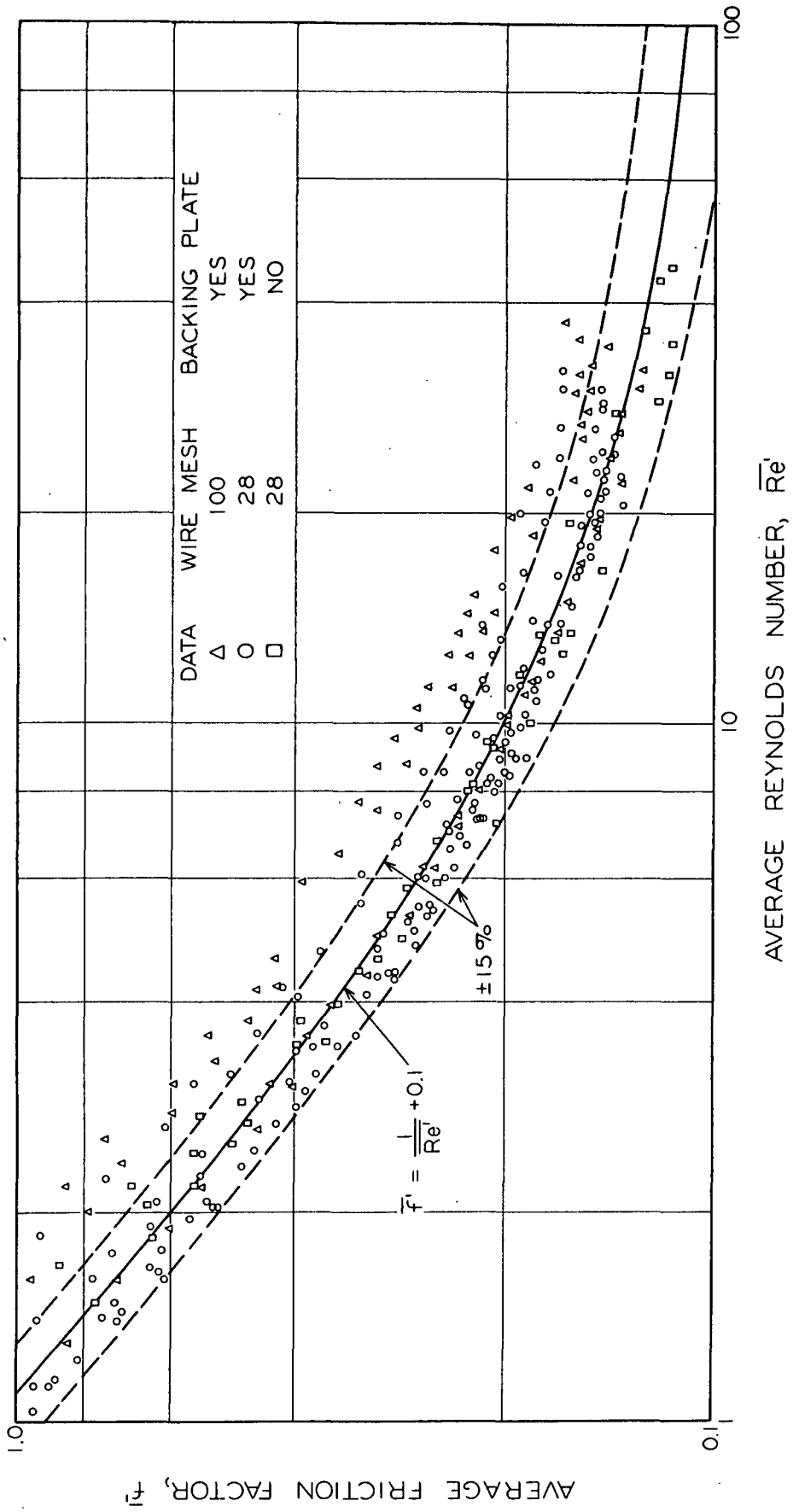


Figure 13. Thin Mat Friction Factor-Reynolds Number Relationship

for basis weights from about 50 to 300 g./sq. m. At higher basis weights, the precision of the experimental data was somewhat better, and the determined deviations have been given previously as ±10% (1).

## Fiber-Wire Interaction

In all cases of significant deviations from the correlation at low basis weights, the experimentally determined pressure drops at given velocities are greater than those predicted from the correlation. The low basis weight results were analyzed in an attempt to explain the deviations. As previously discussed in the Introduction of this report, four possible fiber-wire interaction effects may occur at low basis weights. These effects are summarized in Table III by indicating whether the experimental pressure drops should be either greater or less than those predicted from the correlation. Since all the low-basis-weight deviations are greater than the correlation, it is concluded that the only fiber-wire interactions per se that can account for the results are those of flow convergence in the mat because of the presence of the wire structure, and a more uniform porosity at very low basis weights. The magnitude of the porosity effect may be calculated by assuming a uniform porosity corresponding to the over-all pressure drop. This has been done in Fig. 14 and 15 for the two lowest basis weight curves for the 100-mesh and 28-mesh wires where the deviations from the correlation are greatest. By assuming a uniform porosity, the deviation from the correlation is reduced by about 15% at very low velocities of about 1 cm./sec. where the viscous resistance predominates. At the highest velocities, where the inertial resistance predominates, the deviation may be reduced by about 5%. These estimated corrections for porosity effects at very low basis weights must be considered as the maximum possible corrections. Since a 10-g./sq. m. mat has a thickness of about 3-7 fiber layers,

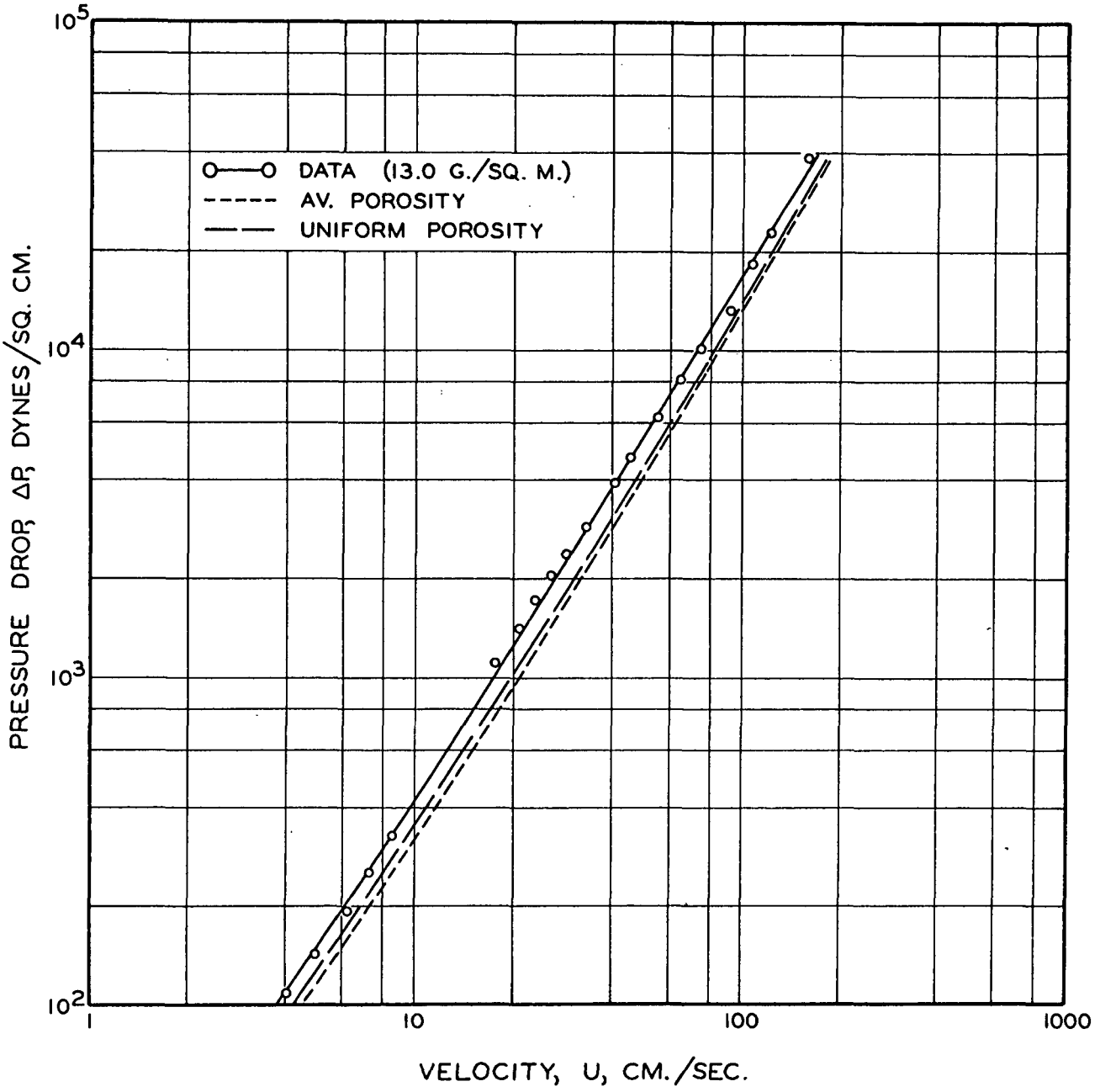


Figure 14. Uniform Porosity Effect of Thin Mats (100-Mesh Wire) on Flow Resistance

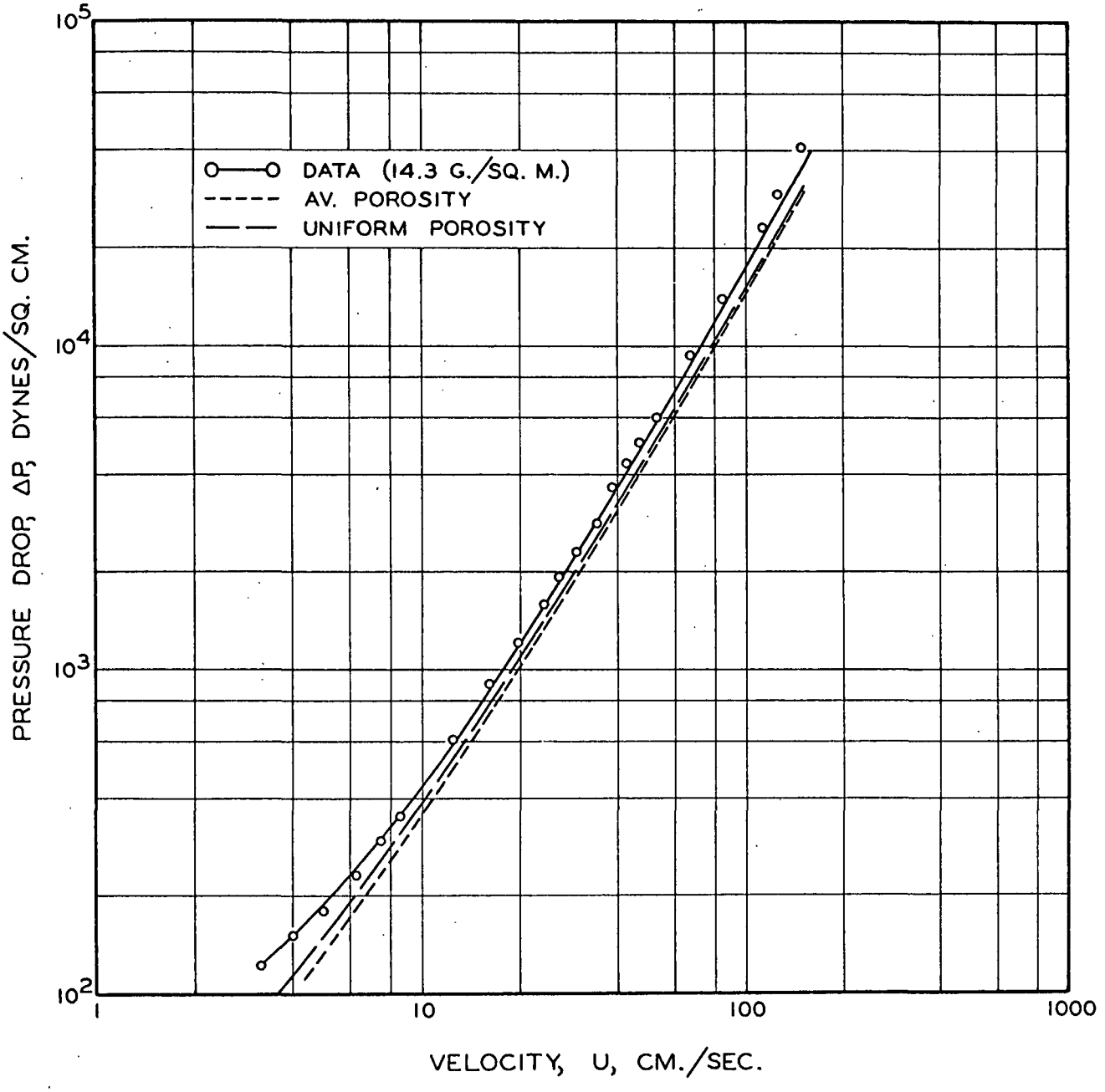


Figure 15. Uniform Porosity Effect of Thin Mats (28-Mesh Wire) on Flow Resistance

TABLE III

FIBER-WIRE INTERACTIONS IN THIN MATS

| Effect | Experimental Pressure Drop Compared to Correlation [Equation (1)] at Same Velocity |
|---|---|
| Flow convergence | greater |
| Porosity distribution | greater |
| Pore-size distribution | less |
| Compressibility | less |

depending upon the over-all pressure drop acting upon it, in the limit a completely uniform porosity would result only for a mat one fiber layer thick. After correcting for porosity, the deviation from the correlation at low velocities is now +15%, and at high velocities is about +20% in Fig. 14 for the 13-g./sq. m. mat on 100-mesh wire. In Fig. 15 for the 14-g./sq. m. mat on the 28-mesh wire, the deviation of the data from the corrected correlation is reduced to about 15%, except for the lowest velocities, where the measured pressure drops were only about 1 mm. of water. The accuracy of the pressure drop measurement at these low values cannot be better than about 25%, and deviations less than this cannot be considered significant.

It appears, then, that only at the highest velocities for very low basis weight mats on the 100-mesh wire do the deviations from the correlation fall 5% outside the 15% limits of all the other data. In this case, it may be possible to have a slightly significant effect of higher pressure drop because of flow convergence in the mat.

The next step in the analysis is to determine why the deviations for thin mats on the coarse-mesh wire were significantly less than those for the

fine-mesh wire. From Estridge's theory (3), the initial retention of the dacron fibers for both the 100 and 28-mesh wires was estimated to be practically complete in the absence of disturbances. However, it was visually observed in the case of mat formation on the 28-mesh wires that there was an appreciable fiber loss in the early stages of mat formation. Therefore, a special material balance was carried out for formation of thin mats on the 28-mesh wires with no backing plate by collecting the filtrate and weighing the unretained fibers. When a 13.6-g./sq. m. mat was formed, the measured fiber loss was 17.3% of the final basis weight. In Estridge's work, the ratio of forming tube diameter to fiber length was about 70, whereas in this study the ratio is only about 14. Since at the wall of the forming tube the fibers will have a tendency to align themselves in the direction of flow, it appears likely that the fiber orientation in the dilute slurry suspensions was not perfectly random but had a preferred orientation of fibers in the flow direction. This effect could account for the high measured loss as compared to nearly complete retention predicted from Estridge's work.

Because of the significant fiber loss in the formation of mats on the 28-mesh wire, it is possible that the resulting structures would have a broader pore-size distribution with a tendency to larger sized pores than in the case of 100% retention on the 100-mesh wires. Since this effect would tend to lower the mat resistance, the discrepancy because of flow convergence would be reduced in the case of the 28-mesh data. This reasoning is qualitatively supported by the results in Fig. 11 and 12 for 28-mesh wire with and without a backing plate, respectively. In the case of 28-mesh with no backing, the fiber loss is greatest, and apparently the counterbalancing of the effect of pore-size distribution now fortuitously gives exact agreement of the correlation and the experimental data at the lowest basis weight studied of 8.1 g./sq. m.

In Fig. 16 and 17, photomicrographs of fiber mats are compared at two basis weights on the 28 and 100-mesh wires. Qualitatively, it may be observed that the maximum pore size on the 28-mesh wire is greater than on the 100-mesh wire. This effect is attributed to the incomplete retention on the coarser wires. For example, the hydraulic radius, $\underline{m}$, of about six of the largest "pores" was measured from the photomicrographs under low magnification. The results showed the average $\underline{m}$ for these largest "pores" was 1100 and 1450 microns for the 13-g./sq. m. mats on 100 and 28-mesh, respectively, and 200 and 800 for the 33.5 and 27.5-g./sq. m. mats on 100 and 28-mesh, respectively. Therefore, it is concluded that the reduction of flow convergence phenomenon in the 28-mesh wire data is indirectly caused by the unexpected incomplete retention.

Photomicrographs in Fig. 16 and 17 qualitatively indicate the possibilities of a decrease in average "pore" size with increasing basis weight and a possible difference in mat compression at low basis weights because of the fewer contact points of the fiber structures on the coarse wire compared to the fine wire. Of course, both of these effects may be occurring simultaneously with the assumed flow convergence and change in structure because of incomplete retention. Rigorous establishment of the presence of the former two effects is possible only through independent determinations of pore-size distribution and compression of thin mats. Although at this time a rigorous separation of the low basis weight phenomena hypothesized in Table III is not possible from permeation data $\underline{\text{per se}}$ because of the interaction of the low basis weight phenomena, it may be safely concluded that the controlling effects (after porosity correction) are flow convergence and change in pore-size distribution because of incomplete retention.

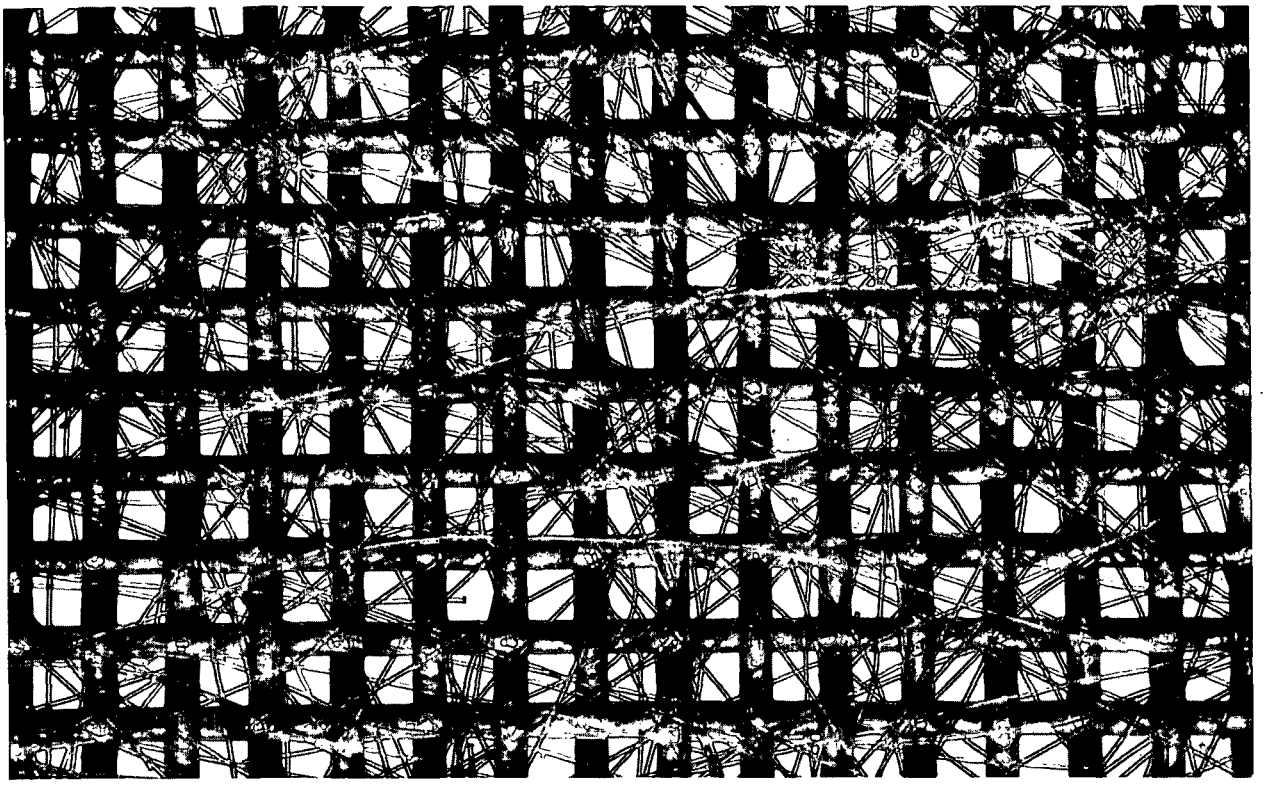

13.6 g./sq. cm. on 100-mesh wire (40X)

13.0 g./sq. m. on 28-mesh wire (40X)

Fig. 16. Thin Mat Deposits on Plain-Weave Wires

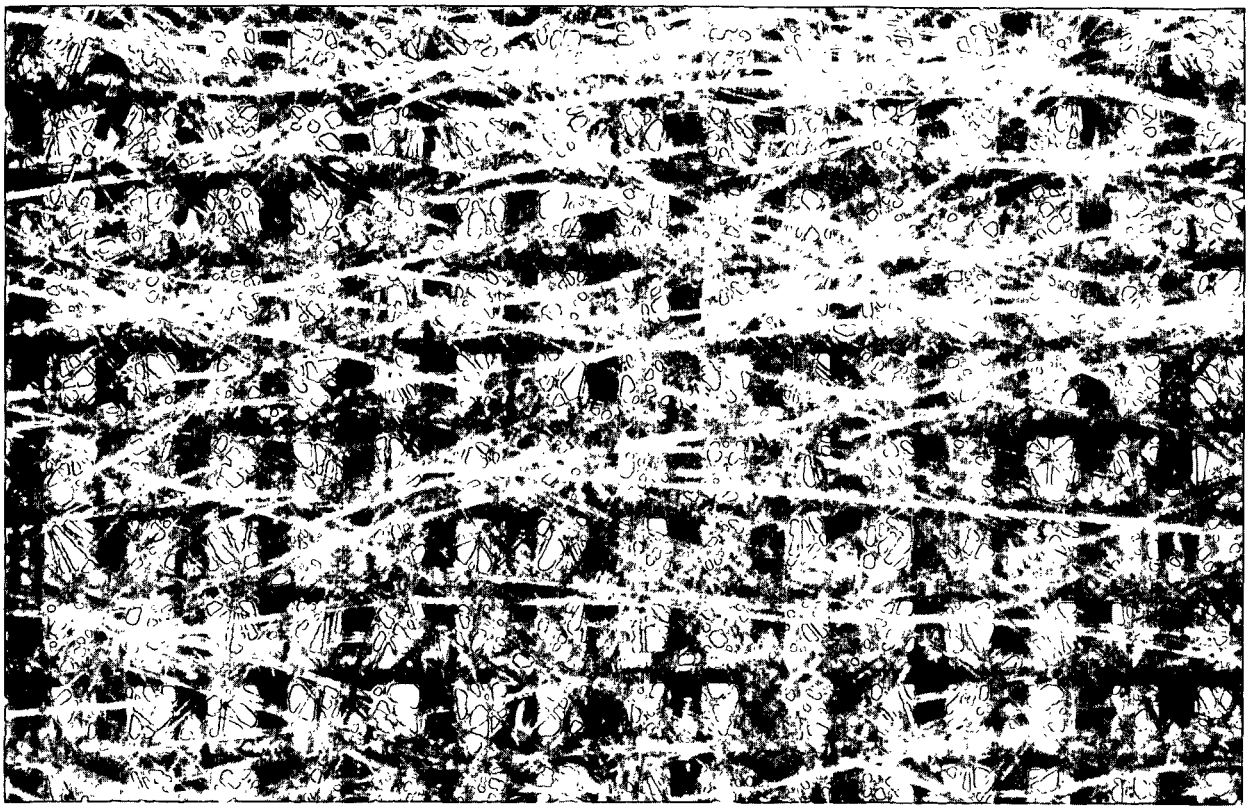

33.5 g./sq. m. on 100-mesh wire (40X)

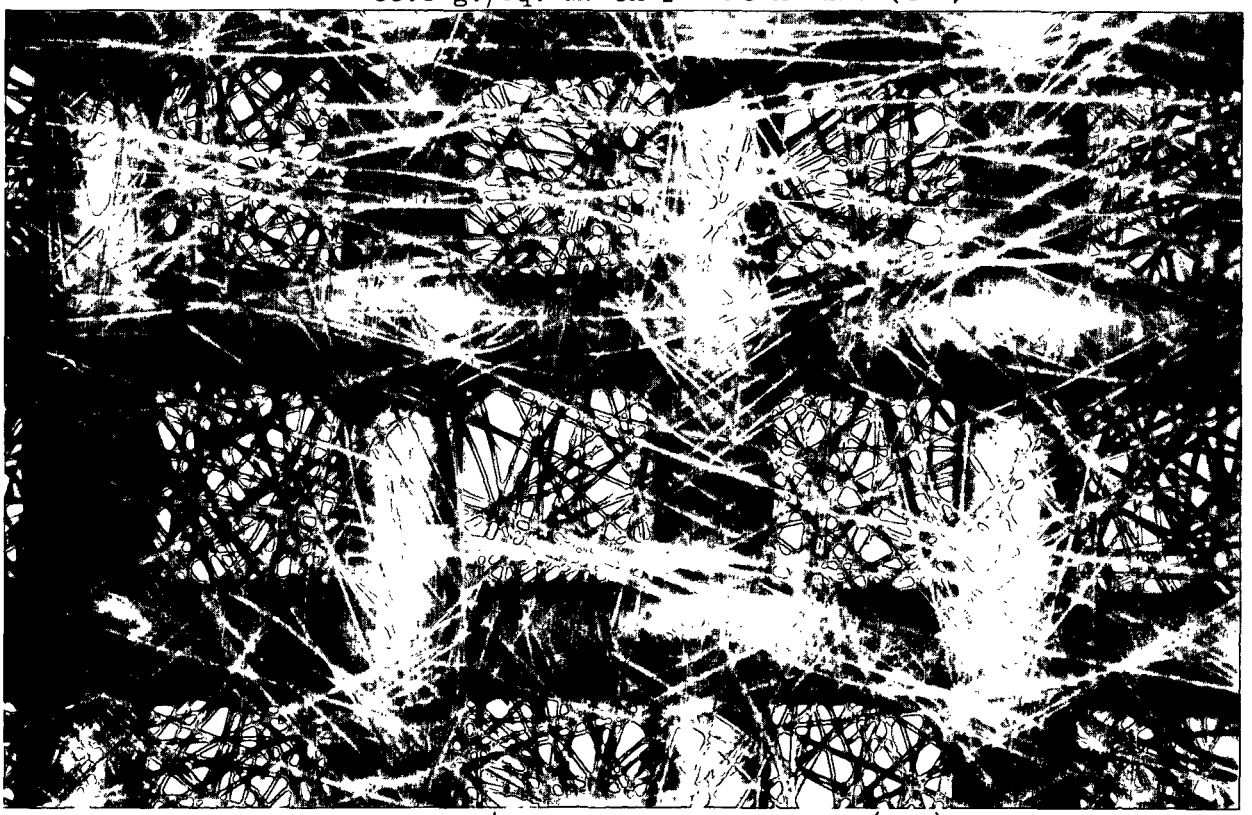

27.5 g./sq. m. on 28-mesh wire (40X)

Fig. 17. Thin Mat Deposits on Plain-Weave Wires

The photomicrographs show the problem involved in rigorously defining the upper and lower boundaries of thin mats because of the significance of fiber diameter in comparison to mat thickness. An attempt was made to provide a geometrically flat surface by studying electromesh screens. The results for a coarse and a fine electromesh screen are presented in Fig. 18 and 19, respectively. Figure 17 clearly shows significant deviations because of flow convergence at high basis weights and a very large effect at low basis weights. By using a finer count of electromesh screen, the effect at high basis weights is reduced but still shows significant deviations at high velocities. Flow convergence is a more serious phenomenon in flat screens because of a greater crowding and bending of flow lines than would be obtained from screens formed from cylindrical wires. Since electromesh screens do not provide any advantage in permeability studies, their use has been abandoned. It appears likely, however, that the electromesh screens will be very useful in future static compressibility tests of thin mats.

Although the maximum velocity of about 160 cm./sec. corresponds to about 5 ft./sec. and represents about the present upper limit of drainage rate for any commercial forming devices, a brief study was made of the validity of the flow correlation at higher velocities. To avoid expensive and time-consuming redesign of the permeation flow system, high-velocity data were obtained by reducing the mat forming diameter from 3 to 1 inch by insertion of a converging 1-in. channel in the flanged forming zone of the Lucite tube. The results of pressure drop and velocity measurements as compared to those predicted from the correlation are shown in Fig. 20 for basis weights from 12 to 90 g./sq. m. The velocity range has been extended from 160 to 450 cm./sec. and no unusual velocity effect was encountered. In general, the correlation lies above the experimental data because of an expected wall effect on mat compression (the

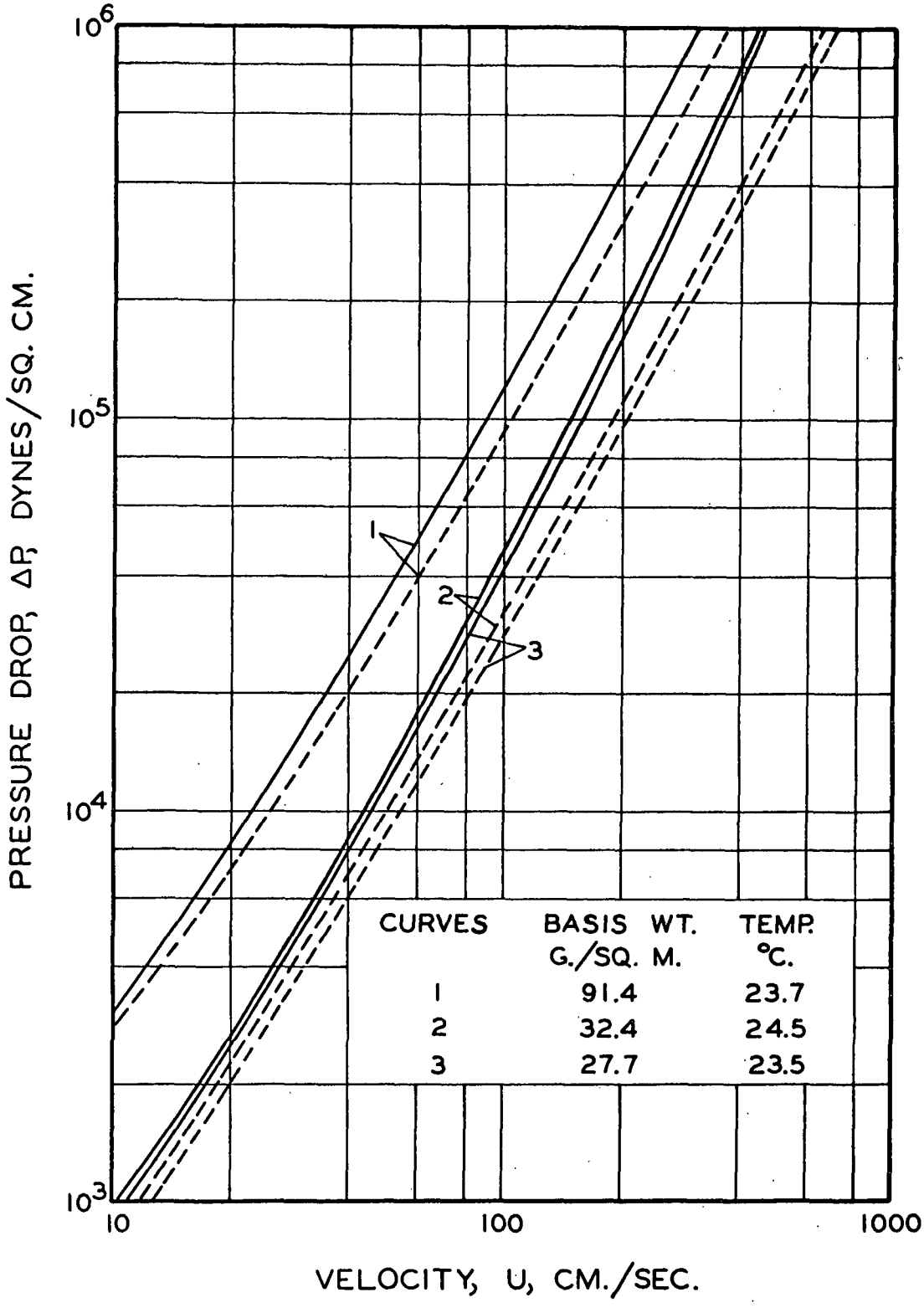


Figure 18. Flow Resistance of Mats on 25-Count Electromesh Screen

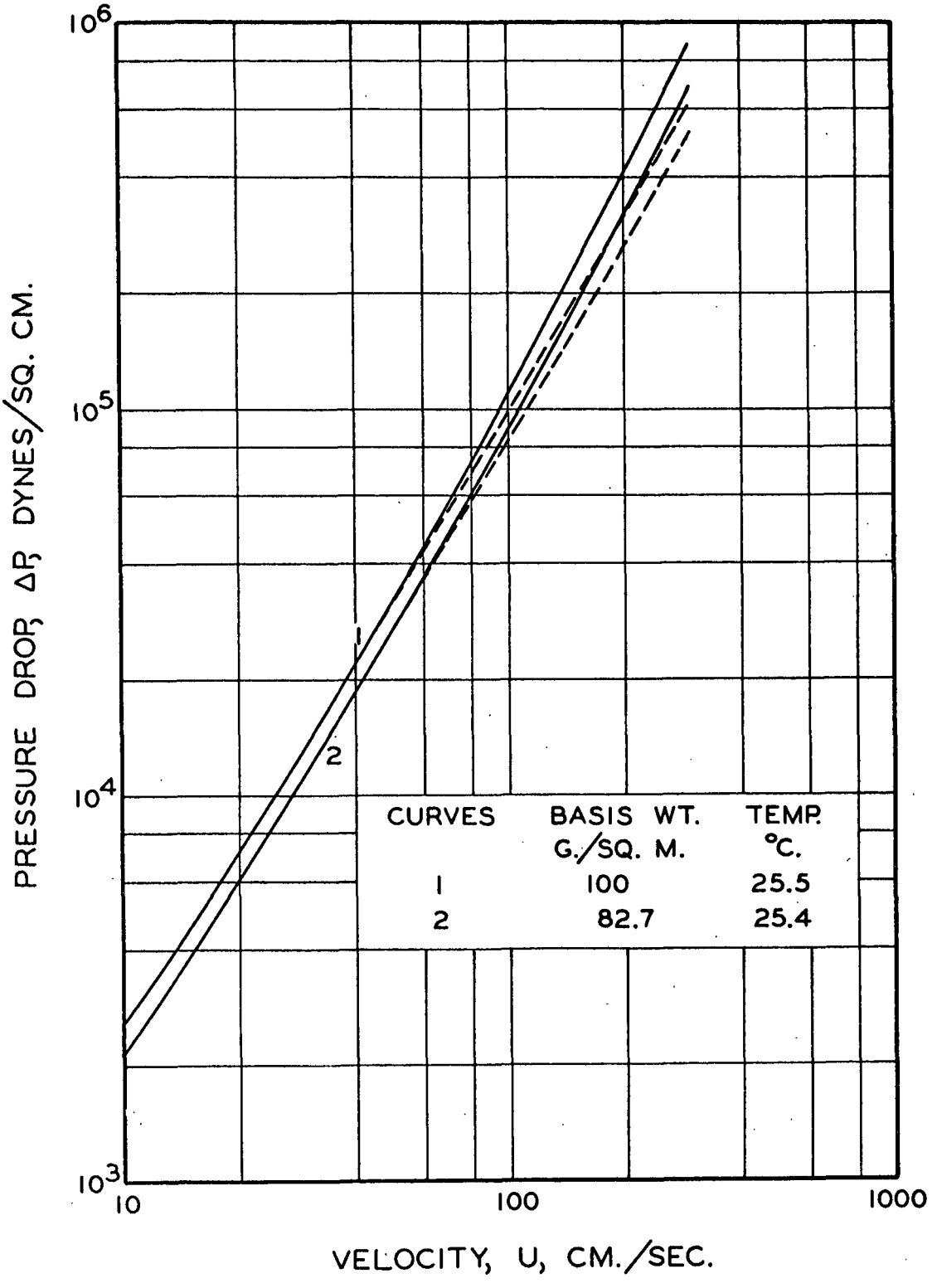


Figure 19. Flow Resistance of Mats on 80-Count Electromesh Screen

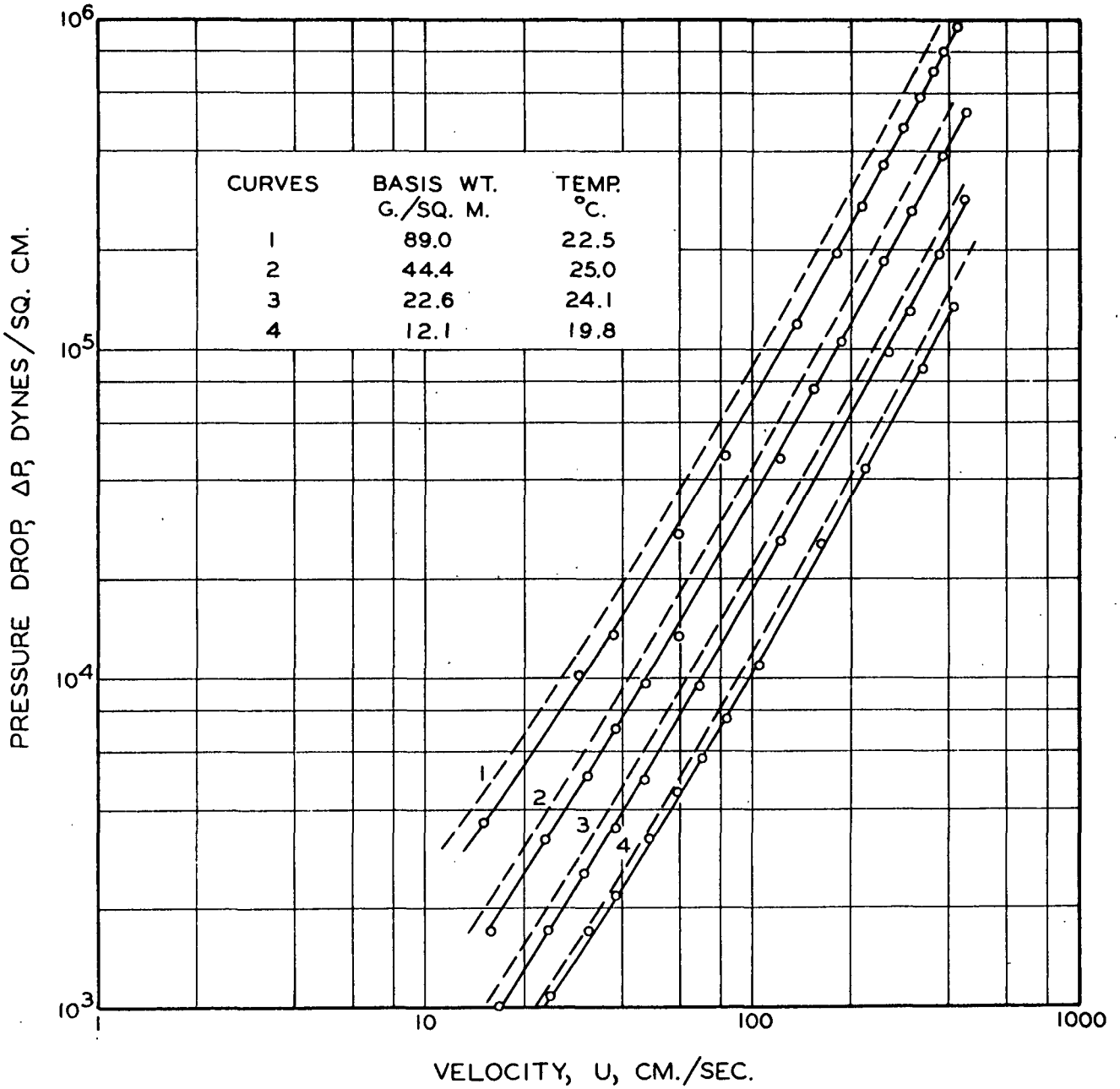


Figure 20. High-Velocity Flow Resistance (1-in. Forming Section, 28 Mesh)

ratio of tube to fiber diameter has been reduced from 17 to about 6). As the basis weights are reduced, the wall effect becomes less important. It is concluded that the velocity range of the correlation may be safely extended to 450 cm./sec.

## CONCLUSIONS

The validity of the flow correlation for thick mats has been established over wide basis weight ranges down to the early stages of mat formation with basis weights as low as 8 g./sq. m. where the wet sheet thickness is only several fiber layers. Four possible fiber-wire interactions may occur at low basis weights below 50 g./sq. m.: (1) flow convergence in the thin mats because of the presence of the forming wire structure, (2) more uniform porosity in mats only several fiber diameters thick, (3) broadening of pore-size distribution with decreasing basis weight or incomplete retention, and (4) change in mat compressibility with decreasing basis weight. The data show that the flow convergence and porosity effects are controlling for mat formation with 100% retention and that changes in pore-size distribution may occur with decreasing basis weight and because of incomplete retention. Because of the interaction of the thin mat flow phenomena, rigorous separation of the effects is not possible without independent determination in special experiments. However, the maximum influence of porosity effects may be quantitatively established, and, when this is done, the flow correlation predicts frictional pressure drop over the mat at a given velocity within $\pm$15% over a 300-fold range of basis weight. The velocity range of the data has been extended beyond present-day commercial drainage conditions to as high as 450 cm./sec., or 15 ft./sec.

## CONTINUING WORK

Because the results of this study have shown only relatively small influence of thin mat phenomena after correction for porosity effects in thin

mats, independent studies of pore-size distribution and compressibility of thin mats as proposed in the objectives of studies of the sheet-forming process will be postponed until investigation of the behavior of wood pulp mats has been studied in high-velocity permeations and filtrations. In addition to these investigations, work has already been initiated on retention of fines in fiber structures. It is anticipated that more significant phenomena may be found in the behavior of more compressible wood pulp fibers as compared to synthetics and in the effect of fines retention on mat permeability.

As noted in Report One (4), dynamic effects of mat compression may occur with compressible wood pulp fibers at high forming rates. In addition, new phenomena in studies of highly swollen and irregularly shaped wood pulp fibers may be encountered, such as nonequilibrium compaction, fiber deswelling, decay of permeability, influence of fiber shape on flow resistance, and non-homogeneity of mat structure because of incomplete fiber and fines retention. It is anticipated that the continuing studies will soon show the relative order of magnitude of these possible effects.

Within the next year's work, it is hoped to initiate preliminary studies of the influence of pore-size distribution and compression of thin mats on wet sheet permeability.

When complicated effects in wood fibers of a considerable magnitude are encountered, it will be necessary to resort again to simplified systems simulating such effects for the purpose of further clarification. With a simpler system, it will be possible to minimize interactions and to develop quantitative treatment. In this way, it is hoped to increase knowledge of the sheet-forming process in a logical manner, keeping practical aspects in mind.

## NOMENCLATURE

$A$ = area, sq. cm.

$a$ = empirical coefficient of viscous wire resistance [Equation (11)]

$b$ = empirical coefficient of inertial wire resistance [Equation (11)]

$c$ = mat density, g./cc.

$d_f$ = fiber diameter, cm.

$\overline{f'}$ = average friction factor, dimensionless

$K$ = Darcy's law permeability coefficient, sq. cm.

$k$ = Kozeny factor, dimensionless; empirical constants, dimensionless

$L_f$ = fiber length, cm.

$M$ = compressibility coefficient, c.g.s. units

$m$ = hydraulic radius, cm.

$N$ = exponent in compressibility function [Equation (8)]

$P$ = pressure, dynes/sq. cm.

$\overline{Re'}$ = average Reynolds number, dimensionless

$S_v$ = specific surface, sq. cm./cc.

$U$ = superficial velocity, cm./sec.

$v$ = fiber specific volume, cc./g.

$W$ = mass of fibers, g.

$y$ = difference between mass of slurry and water-filled pycnometer, g.

$\epsilon$ = porosity, dimensionless

$\mu$ = viscosity, poises

$\rho$ = water density, g./cc.

$\rho_f$ = fiber density, g./cc.

## LITERATURE CITED

1. Ingmanson, W. L., and Andrews, B. D. High-velocity water flow through fiber mats. Tappi, in press.

2. Ingmanson, W. L., and Han, S. T. Permeation. Draft chapter, Project 2348.

3. Estridge, Ronald. The initial retention of fibers by wire grids. Doctoral Dissertation. Appleton, Wis., The Institute of Paper Chemistry, 1962; Tappi 45, no. 4:285-91(April, 1962).

4. Project 2348, Progress Report One, March 1, 1963.

5. Carman, P. C. Flow of gases through porous media. New York, Academic Press, Inc., 1956.

6. Parker, J. D. An investigation of the permeability to water of partially saturated beds of glass fibers. Doctoral Dissertation. Appleton, Wis., The Institute of Paper Chemistry, 1958; Ind. Eng. Chem. 52, no. 3:247-50 (March, 1960).

7. Kallmes, O., and Corte, H. Oxford Conference, 1961, British Paper and Board Makers' Association, in press.

8. Ingmanson, W. L., Andrews, B. D., and Johnson, R. C., Tappi 42, no. 10:840(1959).

9. Wilder, H. D. The compression creep properties of wet pulp mats. Doctoral Dissertation. Appleton, Wis., The Institute of Paper Chemistry, 1960; Tappi 43, no. 8:715(1960).

10. Wilder, H. D. Compression. Draft chapter, Project 2348.

11. Jones, R. L. An investigation of the effect of fiber properties on the compression response of fibrous beds. Doctoral Dissertation. Appleton, Wis., The Institute of Paper Chemistry, 1962; Tappi, in press.

12. Ingmanson, W. L. An investigation of the mechanism of water removal from pulp slurries. Doctoral Dissertation. Appleton, Wis., The Institute of Paper Chemistry, 1951; Tappi 35, no. 10:439-48(Oct., 1952).

13. Ingmanson, W. L., Han, S. T., Wilder, H. D., and Myers, W. T., Jr., Tappi 44, no. 1:47(1961).

THE INSTITUTE OF PAPER CHEMISTRY

W. L. Ingmanson

W. L. Ingmanson

Bruce D. Andrews

B. D. Andrews
Engineering and Technology Section

# APPENDIX I

## FIBER MEASUREMENTS

### MICROSCOPIC MEASUREMENTS

The fibers were dispersed and stained in a 2% water solution of Congo Red dye. The stained fibers were bundled together in parallel orientation and dehydrated by rinsing in increasing percentages of ethyl alcohol (25, 50, 70, 95, and absolute). The fibers were then rinsed with xylene and transferred to xylene saturated with tissuemat for 15 minutes. At the end of this period, they were transferred to 100% tissuemat for approximately 30 minutes and then embedded in the medium. Fiber cross sections 10 microns in thickness were cut with a sliding microtome. The sections were fixed to a slide and placed in a xylene bath to remove the tissuemat and then mounted in Canada balsam in xylene. The projected images (1000X) of the cross sections were traced from the ground glass of a photomicrograph camera and averages computed for diameter measurements. Several diameter measurements of a fiber cross section were made with the aid of a millimeter scale, and the average of each fiber was recorded to the nearest 0.5 micron. Both the arithmetic average and the surface weighted average were computed. The surface weighted average, $\overline{d_f}$, was used to compute fiber specific surface,

$$\overline{d_f} = \frac{\Sigma (d_f)^2_j}{\Sigma (d_f)_j} \qquad (9).$$

For fiber length determination, a small bundle of stained fibers was removed from the original sample and with the aid of dissecting needles the fibers were aligned parallel with one another under a Greenough-type binocular microscope. The measurements were made using a plastic scale fixed upon the

stage of the Greenough scope at a magnification of 15 diameters. About 300 fibers in the bundle were included in determining the average length.

Photomicrographs of the fiber surfaces and the fiber cross sections are shown in Fig. 22.

DENSITY DETERMINATION

The pycnometric density of the fibers was measured in the laboratory using a specially constructed pycnometer, shown in Fig. 21. Conventional pycnometers were not suitable for density measurements of fiber systems because of the problem of sample deaeration.

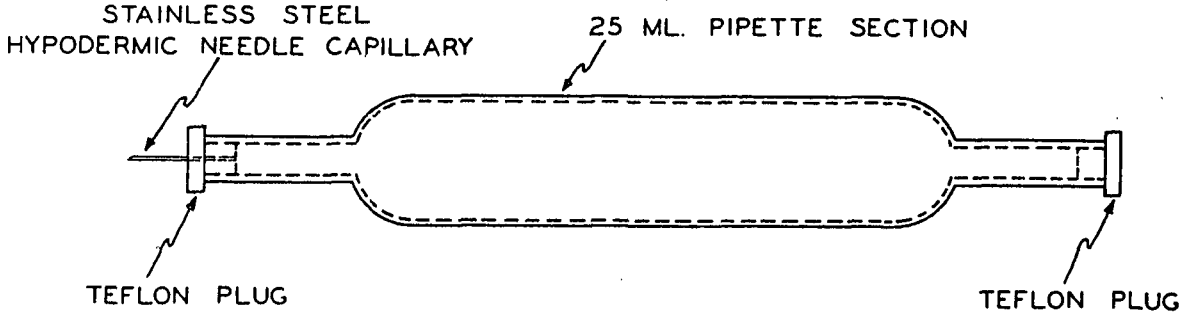


Figure 21. Fiber Density Pycnometer

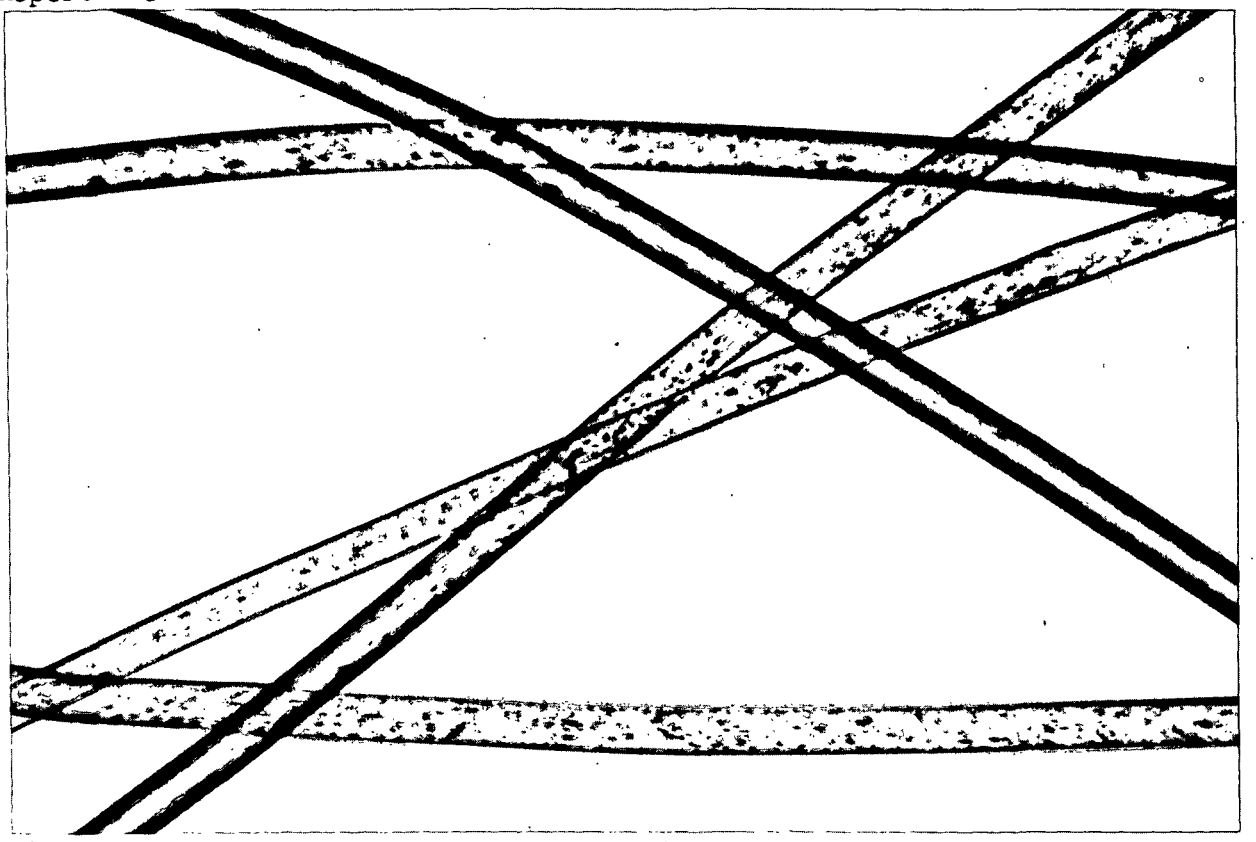

Fiber Surfaces

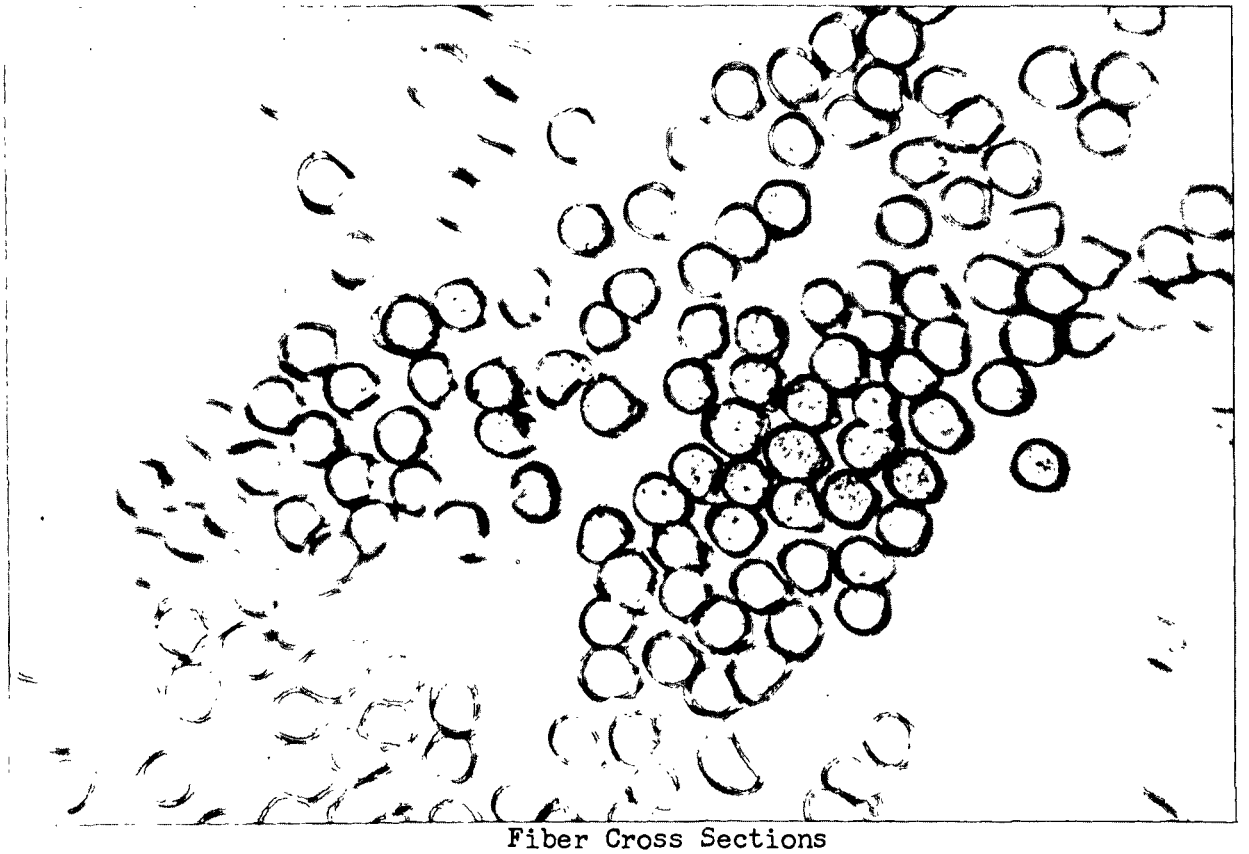

Fiber Cross Sections

Figure 22. 3-Denier Dacron Fibers (340X)

A dilute slurry of the fibers was deaerated over a long period of time under water pump suction and allowed to settle. The high-consistency slurry in the bottom of the container was slowly drawn into the pycnometer through rubber tubing by applying suction. When the pycnometer was filled, the ends of the tubing were clamped off and later the tubing was carefully removed and Teflon plugs inserted.

The densities of the fibers were calculated from the following relationship:

$$\rho_f = \frac{W\rho}{W - y} \qquad (10)$$

where:

$\rho_f$ = density of the fibers,

$W$ = mass of dry fibers,

$\rho$ = density of water, and

$y$ = difference between mass of slurry and water-filled pycnometer.

# APPENDIX II

## WIRE RESISTANCE CORRELATION

The pressure drop and velocity data determined for the bare wires were correlated using a previously established relationship (2, 13) which expresses the pressure drop as the sum of viscous resistance and inertial resistance,

$$\frac{\Delta P}{U} = a + bU^{0.89} \qquad (11),$$

where the empirical constants a and b were determined from graphical representations of the left side of Equation (11) as a function of $U^{0.89}$. These rectified graphs are shown in Fig. 23-25 for 100-mesh wire, and for 28-mesh wire with and without a backing plate. Where minor deviations from the linear relationship occurred, the actual pressure drop data were used to correct for wire resistance.

Photomicrographs of the electromesh screens are shown in Fig. 26.

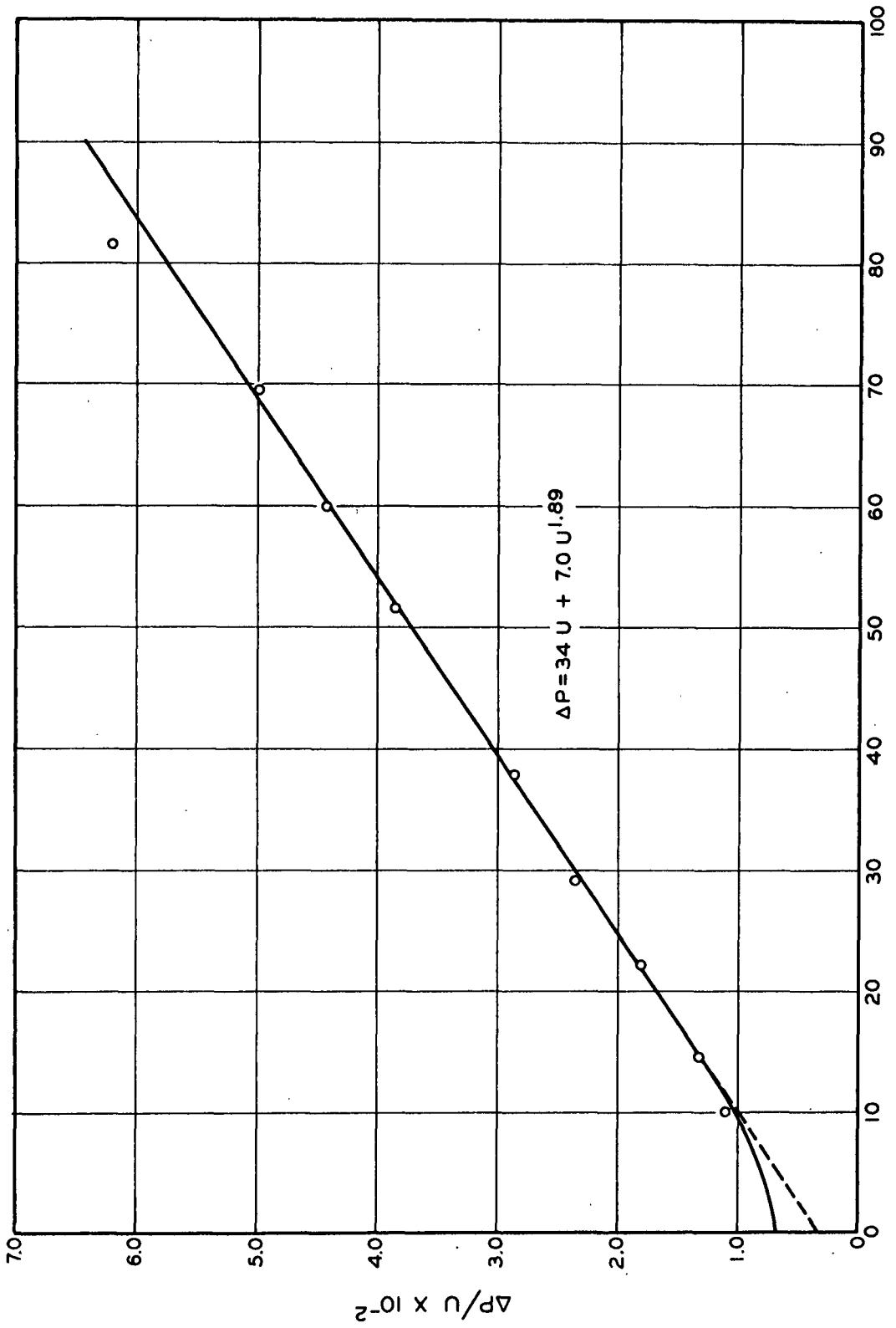


Figure 23. 100-Mesh Wire Resistance Correlation (with Backing Plate)

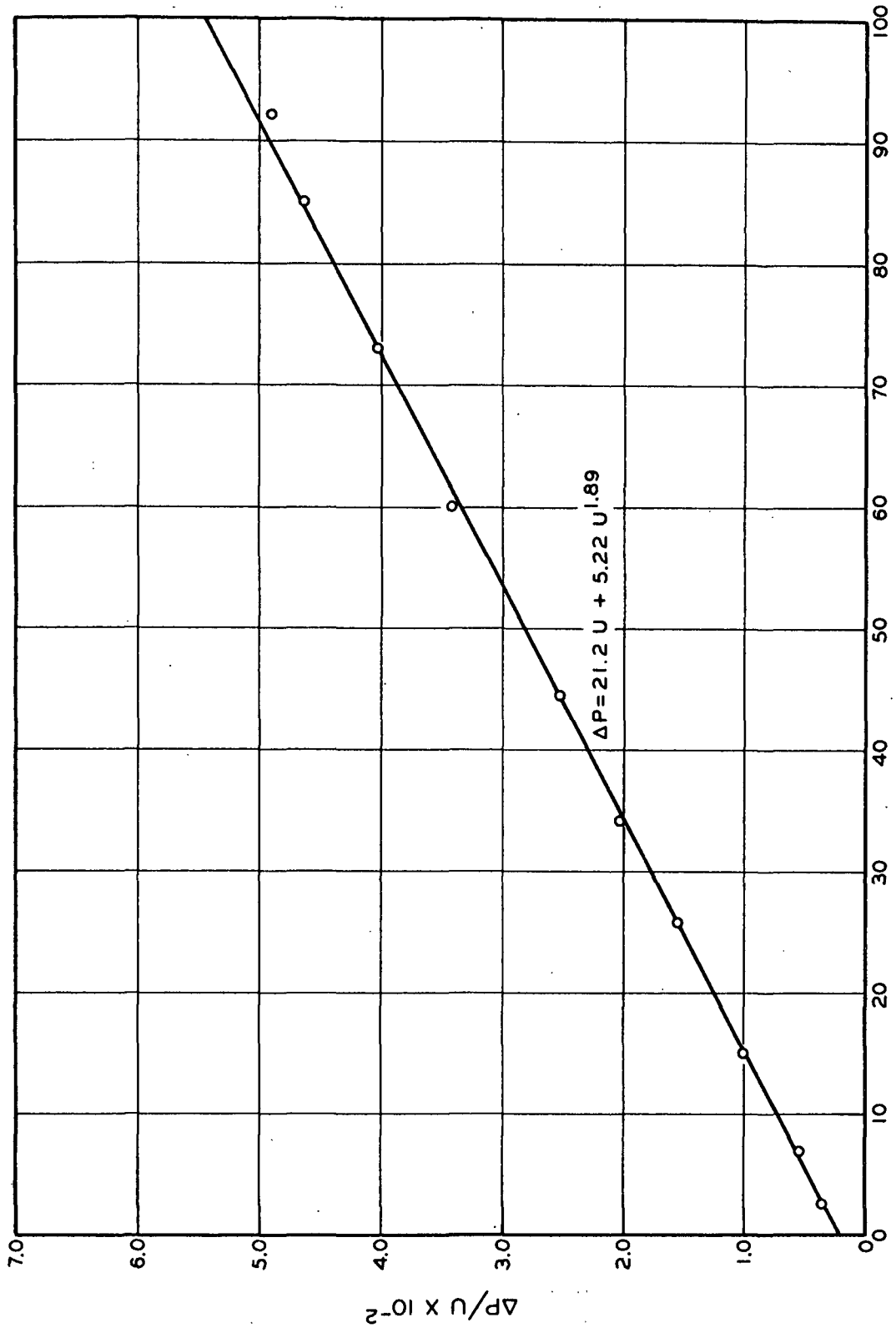


Figure 24. 28-Mesh Wire Resistance Correlation (with Backing Plate)

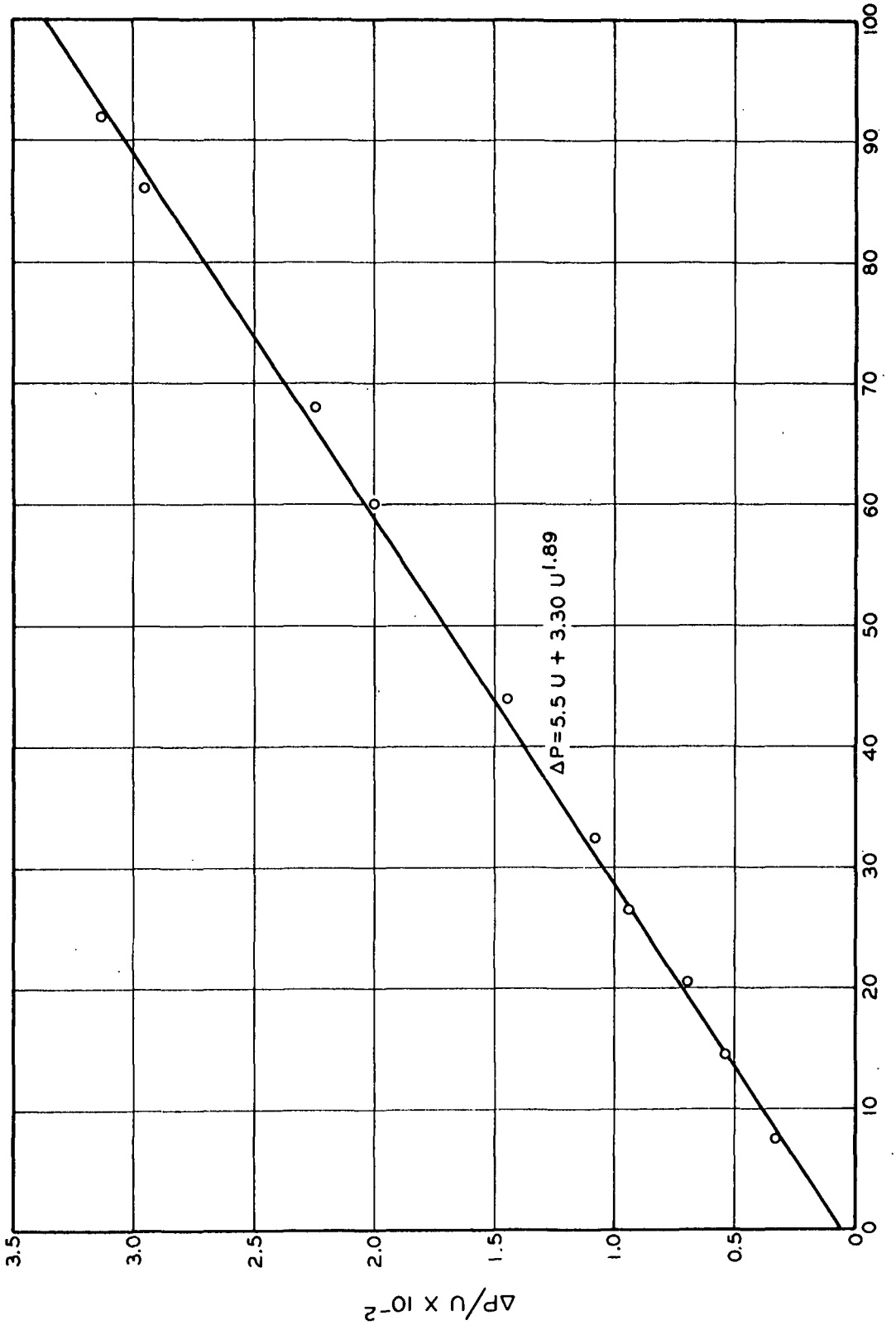


Figure 25. 28-Mesh Wire Resistance Correlation (without Backing Plate)

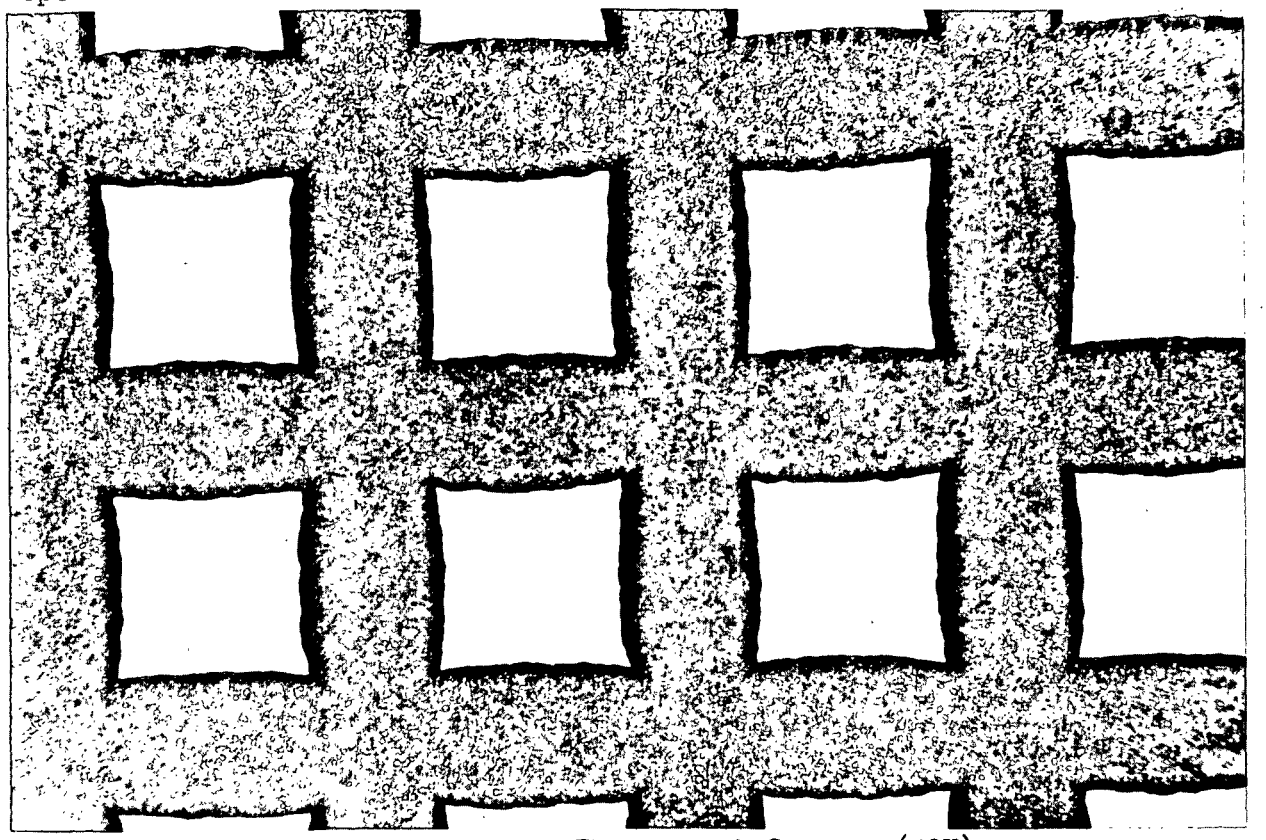

25-Count Electromesh Screens (40X)

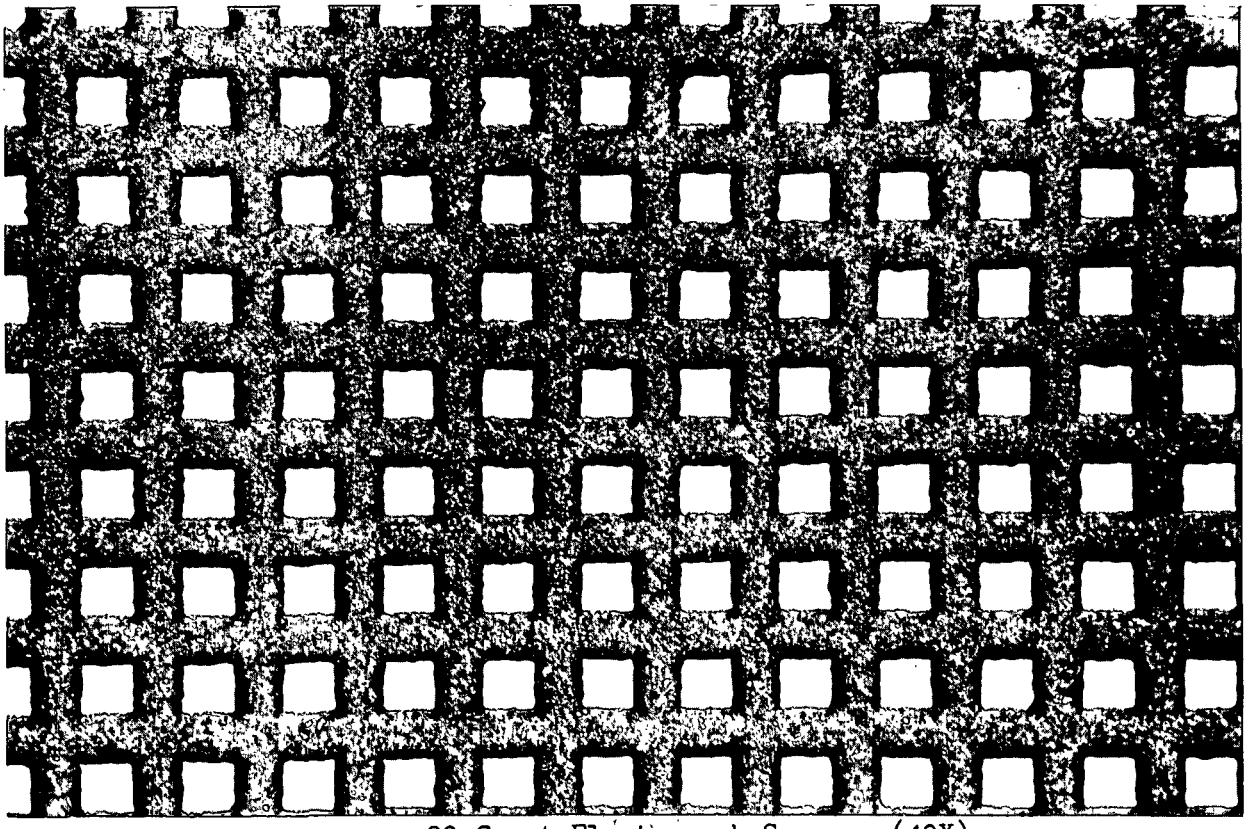

80-Count Electromesh Screens (40X)

Figure 26. Photomicrographs of Electromesh Screens